Received: 29 November 2024 | Revised: 1 May 2025 | Accepted: 11 June 2025

DOI: 10.1002/esp.70117

CASE STUDY

ESPL WILEY

Morphoevolutive drivers on a rapidly-evolving soft rocky cliff and connected shore platform system

Davide Torre[1] | Marta Zocchi[1] | Giulia Iacobucci[1] | Marco Menichetti[2] | Roberto Toselli[1] | Francesco Troiani[1] | Daniela Piacentini[1]

[1]Department of Earth Sciences, Sapienza University of Rome, Rome, Italy

[2]Department of Pure and Applied Sciences, University of Urbino "Carlo Bo", Urbino, Italy

Correspondence
Davide Torre, Department of Earth Sciences, Sapienza University of Rome, P.le Aldo Moro 5, 00185 Rome, Italy.
Email: davide.torre@uniroma1.it

Funding information
RETURN Extended Partnership funding from the European Union Next-GenerationEU (National Recovery and Resilience Plan - NRRP, Mission 4, Component 2, Investment 1.3 - D.D. 1243 2/8/2022, PE0000005), Grant/Award Number: PE0000005

Abstract

Coastal zones, particularly rocky coasts, are increasingly shaped by extreme natural events and processes caused by human activities, making it essential to understand the key drivers guiding their evolution. This study examines the soft rocky coast and shore platform system of Tor Caldara Natural Reserve, a site of natural, archaeological and touristic significance. The research aims to identify the drivers that influence erosion, including lithology, rock mass properties, marine wave action, slope morphology and rainfall. A comprehensive approach combining traditional field surveys, multi-temporal Unmanned Aerial Vehicle (UAV) acquisition and multispectral analysis of high-resolution satellite imagery was employed to conduct a detailed analysis of geomorphic changes in the last 15 years. Marine and meteorological datasets were analysed to assess the impact of wave action and precipitation on coastal erosion. Wave height data were correlated and subjected to Peaks Over Threshold (POT) analysis to identify the peaks, corresponding to independent events, that could potentially impact the cliff. Rainfall data were also examined to evaluate whether precipitation intensity has played a significant role in accelerating cliff instability. The study reveals a dynamic and rapidly evolving coastal environment (in some local points about 1 m/yr of retreat of the cliff) characterized by both continuous and abrupt changes. Analysis of drivers controlling morphoevolution suggests that while marine and continental forcing play preparatory roles, the cliff setting, including lithology and structural conditions, is fundamental in driving coastal evolution at the study site. The evaluation of temporal mesoscale processes shaping the rocky coastline contributes to a better understanding of erosion processes affecting soft rocky coasts, serving as a basis of future research aimed at improving coastal management and risk mitigation strategies.

KEYWORDS
coastal erosion, field survey, morphoevolution, rock fall, rocky coast, UAV

1 | INTRODUCTION

Nowadays, coastal zones, which are among the most dynamic and economically significant regions on Earth (Martínez et al., 2007), are experiencing a global increase in coastal hazards due to intense human activity and the impacts of global changes (Aucelli et al., 2018), considering also the future projection scenarios of the sea-level reported by the Intergovernmental Panel on Climate Change (IPCC, 2021). Rocky coasts constitute about half of the world coasts and those of the Mediterranean (Furlani et al., 2014; Young & Carilli, 2019); in particular, along the Italian peninsula are approximately 36% of the natural coasts (Trigila et al., 2021). In recent years, these coasts have seen an increase in studies, compared to the more extensively studied low-lying coasts. This increased attention

coincides with significant advancements in technology and remote sensing analysis techniques (Cavalli, 2024), which has enabled the use of growing amounts of remote data and analyses for the study of rocky coasts (Fullin et al., 2024; Piacentini et al., 2021). However, to gain a comprehensive understanding of the geomorphic processes shaping rocky coasts over extended time frames and across larger scales, remote sensing analyses must be complemented by field observations (e.g. the geomorphological and geological interpretation covered by Torre et al. (2024). The employment of Unmanned Aerial Vehicles (UAVs) for coastal monitoring and characterization is continuously growing (Devoto et al., 2020; Francioni et al., 2018; Fullin et al., 2023; Furlani et al., 2022; Tursi et al., 2023), through which Digital Elevation Models (DEMs) with centimetre resolution, point clouds and images can be obtained. To quantitatively determine geomorphic changes, DEM of Differences (DoDs, James et al., 2012) method is commonly used today, though it is limited to a raster analysis in a 2D plane. To analyse all three dimensions, scalar field algorithms can be employed to compare point clouds obtained from UAV photogrammetric or Light Detection And Ranging (LiDAR) surveys (Esposito et al., 2017; Vanneschi et al., 2017). Finally, high-resolution optical and multispectral satellite imagery offer an incomparable dataset for detecting and mapping changes, especially when multi-temporal acquisitions with short revisit periods are freely available (Piacentini et al., 2021; Turner et al., 2021). The evolution of rocky coasts is determined by the interaction of various drivers (Sunamura, 1992; Trenhaile, 2011), such as waves action (Kennedy, Paulik, & Dickson, 2011; Poate et al., 2018; Sunamura, 2015; Young et al., 2021), cliff attitude and the rock mass properties (Fullin et al., 2024; Marmoni et al., 2023; Prémaillon et al., 2021; Troiani et al., 2020) and coastal landslide activity with intense rainfall or erosion due to thermo- and cryo-clastism (Cevasco, Pepe, & Brandolini, 2014; Lim et al., 2020; Strzelecki et al., 2017; Young et al., 2021). Understanding the erosional drivers that control time and style of the evolution is crucial for implementing appropriate risk mitigation strategies. This involves analysing and distinguishing the roles of predisposing (time-independent), preparatory (time-dependent) and triggering (transitory) factors (Delchiaro et al., 2024) and the different combinations of these can result in either short-term or long-term evolution.

In this study, a sector of the Thyrrenian coast close to the Anzio municipality (Italy), within the limit of the Tor Caldara Natural Reserve, a Site of Community Interest, is examined, with the aim of determining the drivers that influence its evolution. This coastal sector is one of the few examples of a soft rocky cliff and shore platform system occurring along the Thyrrenian coastline of Italy, with an emergent shore platform that is easily accessible. In fact, along the Tyrrhenian coast other shore platform systems are present, featuring hard lithologies, such as limestones with lower erosion rates, or with a submerged platform (Furlani et al., 2014). The whole coastal cliff is in general characterized by gravitational instability phenomena which affect not only an area of summer tourism but also a natural and archaeological heritage site.

In this context, the analysis of various drivers in the coastal stretch of interest, such as lithology and rock mass compactness, marine wave action, slope morphology and precipitation, plays an important role in evaluating which drivers are guiding morphoevolution. Through the analyses conducted in this study, which integrate field with repeated UAV surveys and multispectral satellite investigation. It is possible to aid the development of models and enhance the understanding of the evolution of the soft rocky coast at the mesoscale (Walkden & Hall, 2005), i.e., over longer time periods.

Although this study focuses on a specific coastal stretch, its finality is to provide a complete methodological approach offering a scalable framework, which integrates UAV photogrammetry, multispectral satellite imagery and field surveys, useful for investigating soft rocky coasts globally. Understanding erosional drivers is essential for assessing coastal vulnerability and developing effective mitigation strategies, making this research a valuable reference for coastal monitoring and management in a similar context.

Starting with an overview of the study area, detailing its geographic and geological characteristics, the instruments and the methods used for both field surveys and UAV-based analyses are explained. Following this structure, the results are supplemented by the application of the Digital Shoreline Analysis System of USGS (DSAS) on satellite-derived cliff crests (SDCC), and the statistical analyses of the meteo-marine data. Hence, the mean retreat rate in the last 15 years and the main drivers influencing this rocky coastline are provided.

2 | STUDY AREA

The coastal sector of Tor Caldara (41°29′12“ N, 12°35’21” E, Figure 1) is a 700 m long coastal cliff with an elevation of about 15 m above sea level (a.s.l.) and is located in the province of Rome (Lazio, central Italy). The cliff is included in the Regional Natural Reserve of Tor Caldara, with an area of about 1.56 km^2, established by the L.R. 50/1988 and later declared a site of Community interest with the D.M. 157/2005. The reserve area also aligns with the Natura 2000 site IT6030046, which was designated as a Special Area of Conservation (SAC) in 2016 (Pantaloni et al., 2020). Thanks to the presence of sulphurous emissions, the reserve has not undergone major changes with the urban development of the last two centuries, which is clearly visible beyond the limits of the reserve itself (Figure 1) with the Lavinio-Lido di Enea to the N and Lido di Cincinnato to the S. The scarcity of urbanization along the coast of the Natural Reserve attracts many people, especially in the summer months.

The coastline shows a general NW-SE orientation, with a small local variation due to an extension of the cliff towards the sea in the central portion, caused by the presence of a seaward adjacent shore platform. The area is characterized by a semi-humid, temperate Mediterranean climate, i.e. Csa typology according to Köppen-Geiger classification (Beck et al., 2018; Fratianni & Acquaotta, 2017), with hot and dry summers and humid winters. The annual precipitation reaches values of about 700 mm and the mean daily temperature values are about 16°C (Colantoni et al., 2015) with values of 26°C and 8°C, as maximum and minimum mean monthly temperatures reached respectively in August and January. Dominant winds approach from W-SW with a speed up to 15 m/s, and waves present a significant wave height of about 3.9 m and a wave period of 9 s calculated for the period 1951–2011 by (Mastronuzzi et al., 2017) (Figure 1). The average semi-diurnal syzygyal tidal range is about 0.3–0.4 m and the prevailing longshore current flows towards the N (Di Bella et al., 2020).

2.1 | Geological and geomorphological setting

The study area is located along the Tyrrhenian margin of the Central Apennines, where tectonic processes, sea-level variations and volcanic activity have shaped the present-day landscape over time (Mancini, Bellucci, & Petronio, 2008; Marra et al., 2019). It is considered one of the westernmost extensions of the Colli Albani volcanic complex (D'Angelo et al., 1999), even though the cliff between Tor Caldara and Anzio reveals a 100-m-thick Plio-Pleistocene succession, made up of both marine and transitional litho-facies (Pantaloni et al., 2020). The outcropping formations are well described by Bellotti et al. (1997), who divide them into four informal Units (here described from the oldest to the most recent) (Figure 2): (i) Unit 1 (lower Pliocene) consists of greyish clayey pelites and is found only in the southern part of the coastal sector under study, with an almost sub-horizontal bedding, then continuing towards Anzio with a bedding of N 20–30°E; (ii) Unit 2 is characterized by a yellowish bioclastic calcarenite and is found only outside the study area towards the city of Anzio; (iii) Unit 3 (lower Pleistocene) crops out discontinuously and is composed of greyish to yellowish cemented sands and clayey sands (Di Bella et al., 2005). At Tor Caldara cliff, this Unit with a thickness of about 5 m, is interbedded with two grey pelitic layers of approximately a maximum

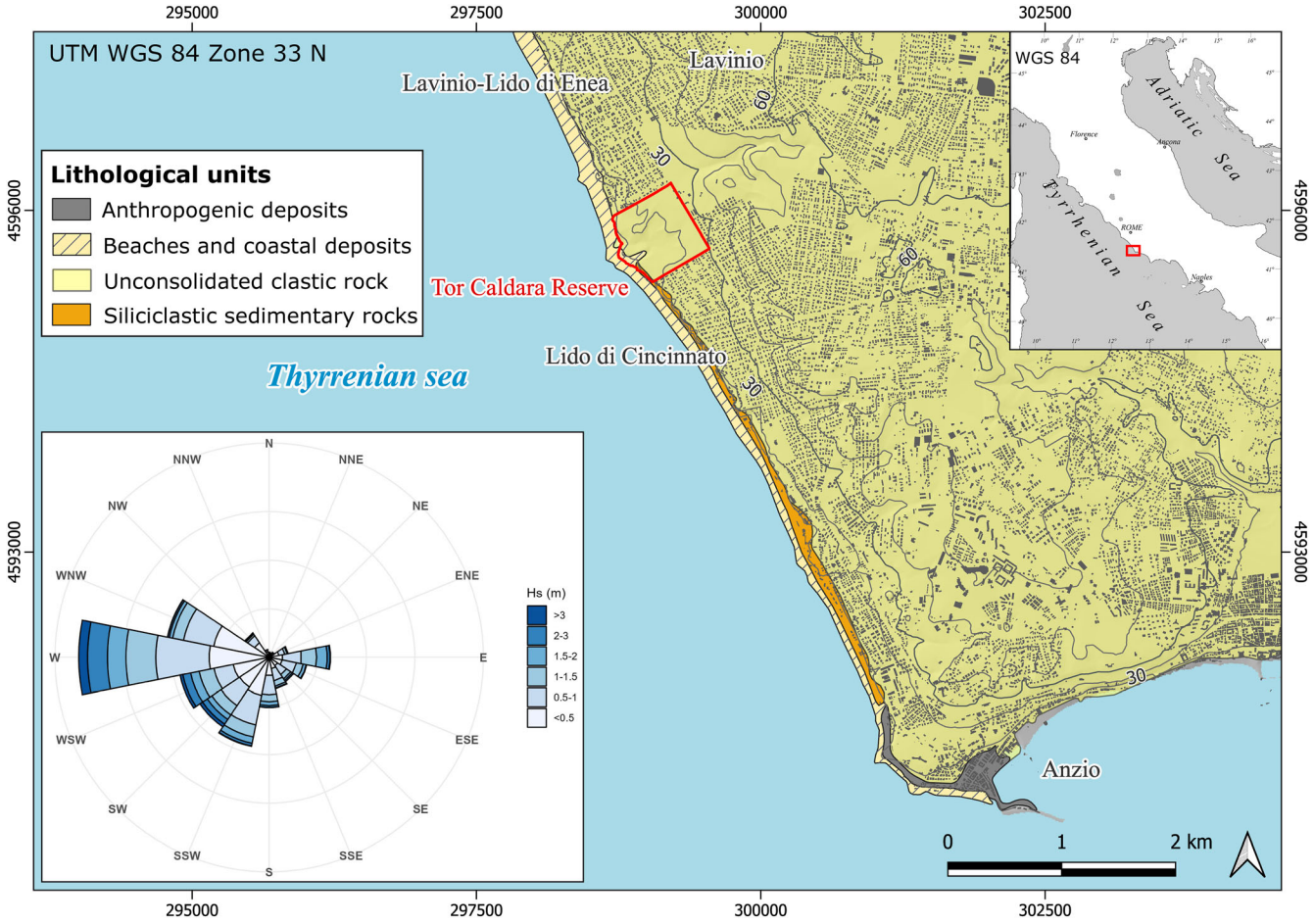

FIGURE 1 Lithological setting map of the northern coastal sector of Anzio municipality (lithology modified after Bucci et al. (2022). Tor Caldara reserve limits are shown with the red polygon, along the coastline. The waves diagram was redacted from the data available on the website of the Ponza wave buoy (ISPRA, 2024) and illustrates the wave directions and heights for the period from 2019 to 2024.

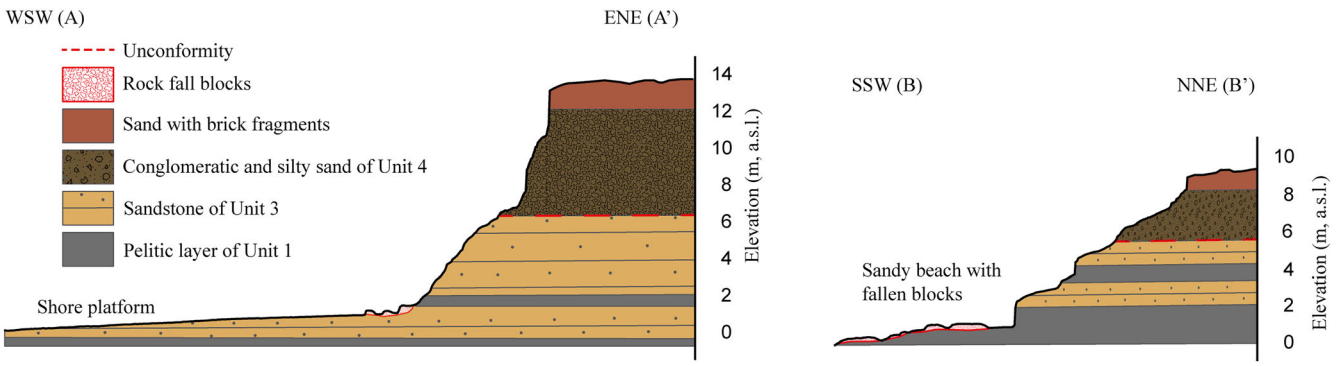

FIGURE 2 Schematic geological sections of the tor Caldara coastal area. Profile traces are represented in Figure 4.

50 cm each one. The bedding is sub-horizontal, and the contact with the previous Units is dislocated and unconformable. Additionally, abundant shells of *Arctica islandica* (Linnaeus 1767) are found in the basal part; (iv) Unit 4 (middle Pleistocene) consists of conglomeratic sands at the base and silty sands towards the upper part. It has a minimum thickness of 8 m and is in contact with Unit 3 at the base through an erosion surface, while the upper boundary is overlain by reddish sands with brick fragments. In the central part of this Unit, bidirectional cross-lamination is observed. All the coastal sectors of Anzio constitute a structural high (Faccenna et al., 1994), morphological expression of the post-orogenic extensional regional tectonics, which extends from the coast up to the volcanic complex of the Colli Albani. The main structure is an anticline with a SW–NE trending axis, culminating near Tor Caldara (Mancini, Bellucci, & Petronio, 2008). Along the Latium Tyrrhenian margin, the tectonic uplift rate has been estimated to be approximately 0.224–0.230 mm/yr (Milli et al., 2016 and reference therein; Marra et al., 2023) over the last 300–125 ka. Historical gravitational instability phenomena, including planar, rotational and fall typologies, have already been identified along the entire cliff stretching from Tor Caldara to Anzio (D'Angelo et al., 1999).

The Tor Caldara area is characterized by gas emissions that are likely connected to the volcanic complex of Colli Albani through a system of tectonic lineaments, which provide a preferential pathway for the ascent of fluid and gases (Mancinella, Mantero, & Testardi, 2020). The structural lineaments on the coastal area are oriented approximately NE–SW in the northern part and E-W in the southern part, with degassing vents aligned along their extension (Carapezza et al., 2019). The gas emissions have been observed not only inland and above the cliff, but also on the seabed in front of the Natural Reserve, and they are also aligned along preferential directions (Mancinella, Mantero, & Testardi, 2020). The area experienced intense sulphur mining activity in the 15th and 16th centuries, which significantly altered the natural landscape of the sulphur springs (Mantero & Giacopini, 2020). Since 1990, the National Institute of Geophysics and Volcanology (INGV, 2024) has recorded six seismic events in this area with a magnitude greater than 3, including a magnitude 4.6 event on August 22, 2005, during which a variation in gas emissions was observed (Carapezza et al., 2019).

3 | MATERIALS AND METHODS

The geomorphological analyses conducted in this work were based on an integration of traditional field-based geomorphological surveys and remote sensing techniques, using UAV and high-resolution satellite images. For a correct interpretation of the evolutionary dynamics, meteo-marine data for the Anzio coast were also collected, specifically wave height and daily precipitation, covering the period from 2019 to 11-25 to 2024-07-31.

3.1 | Field surveys data collection and GIS analysis

Geomorphological field surveys were conducted approximately every three months to map landforms and observe any changes that occurred after storm events. Rock mass properties were evaluated, in the field, with measurements of discontinuity orientations and of the Uniaxial Compressive Strength (UCS), derived from the number of rebounds recorded with a Schmidt Hammer for the different lithologies. Through these surveys, a comprehensive geomorphological map was also prepared to identify the different landforms present in the area, particularly the extension of the shore-platform. Historical aerial images and DEMs, analysed using QGIS 3.34.4 open-source and ArcGIS Pro 3.2.2 software (ESRI®, 2023–2024-licensed Sapienza University of Rome), have also been useful for accurately identifying the extent of the shore platform and mapping features such as rock fall deposits, which were later covered by sand. The DEM dataset includes a LiDAR Digital Terrain Model (DTM), provided by the Ministry of the Environment and Energy Security of Italy (Geoportale MASE, 2024), with a ground resolution of 2 m and an altimetric accuracy of ± 0.15 m. The basic geological map at a scale of 1:25.000 is available in vector format on the Geoportal of the Lazio region (Geoportale Regione Lazio, 2024). The typology of rocky coasts was designated using the classification proposed by Sunamura (2015) and the gravitational phenomena mechanism according to Hungr, Leroueil, & Picarelli (2014).

3.2 | UAV surveys and photogrammetric analyses

Field surveys were supported by UAV flights to acquire multitemporal images with two different types of drones: DJI Mavic 2 Pro (M2P) and DJI Mavic 3 Enterprise (M3E). One of the differences between the two drones lie in the optical sensor, which is superior in the M3E. The M2P is equipped with a 20 MP Hasselblad camera featuring a 1" CMOS sensor. The camera is fastened on a 3-axis gimbal for image stabilization and has an equivalent focal length 28 mm, a field of view (FOV) of ca. 77° and an aperture of f/2.8-f/11. Similarly, the M3E is equipped with a 20 MP Hasselblad camera but with a larger 4/3" CMOS sensor. This camera is also stabilized by a 3-axis gimbal and features an equivalent focal length of 28 mm, a slightly wider FOV of ca. 84° and the same aperture of f/2.8-f/11. Furthermore, both drones are equipped with an electronic shutter (8–1/8000 s), while only the M3E also features a mechanical shutter (8–1/2000 s).

The main difference is that the M3E mounts a Real Time Kinematics (RTK) sensor for photograph georeferencing, offering horizontal and vertical accuracies of about 1 cm and 1.5 cm respectively, under optimal field conditions. For the M2P drone, which lacks an RTK sensor, we used an EMLID Reach RS2 + (multi-band RTK Global Navigation Satellite System, GNSS) receiver to measure Ground Control Points (GCPs) uniformly spread throughout the study area. Nonetheless, it was deemed appropriate to input the coordinates of some fixed point, taken to the N of the study area with the previously used GNSS station, to achieve better accuracy as suggested by the study of Štroner et al. (2020). The estimated georeferencing errors, split into various directions, are provided in the following Table 1 for both the survey conducted with the GNSS station and the integrated RTK sensor of the second drone:

The photogrammetric surveys were programmed and performed using the UgCS EXPERT (SPH Engineering, 2023-licensed University of Urbino "Carlo Bo") software, which allows to make automatic flights of a predefined area based on the desired ground resolution

TABLE 1 Estimated errors for the two georeferencing methods calculated on Agisoft Metashape.

	Latitude (Y) error (m)	Longitude (X) error (m)	Altitude error (m)	XY plane error (m)	Total error (m)
EMLID Reach RS2 + (first survey)	0.041	0.047	0.033	0.063	0.071
Mavic 3 RTK sensor (last survey)	0.03	0.02	0.02	0.037	0.041

TABLE 2 The satellite dataset adopted in the present work.

Acquisition date	Satellite mission	Spatial resolution	Spectral resolution (nm)
04/15/2009 04/09/2012	RapidEye (RE)	5 m	5 bands Blue: 440–510 Green: 520–590 Red: 630–685 Red Edge: 690–730 NIR: 760–850
05/20/2018 05/11/2021	PlanetScope (PS)	3 m	4 bands Blue: 455–515 Green: 500–590 Red: 590–670 NIR: 780–860

(ca. 0.02 m). To achieve centimetre-level resolution and enable comparison between different surveys all flights were conducted at the same altitude (approximately 75 m a.s.l.) utilizing the UgCS skill of the terrain follow based on a reference DTM. The LiDAR DTM from the Ministry (Geoportale MASE, 2024) was chosen as the base DTM. Images were captured with a forward overlap (along the flight strip direction) of 80% and a side overlap of 70%. The flight speed ranged between 3 and 4 m/s to mitigate rolling shutter effects (Stark et al., 2021), and the optical sensor tilt was approximately 86°. In addition to these flights, automatic flights at higher altitudes (around 100 m) and manual flights with both frontal and oblique images relative to the cliff face, were also executed. The collected images were elaborated using Structure-from-Motion (SfM) algorithm through the Agisoft Metashape 2.1.0 (Agisoft, 2024-licensed "DST Sapienza University") software, to generate point clouds, Digital Surface Models (DSMs) and orthophotomosaics, according to the workflow suggested by (Over et al., 2021; Turner, Harley, & Drummond, 2016). The workflow involves: (i) quality correction of the images, if necessary, (ii) photo alignment, (iii) insertion of GCPs if required, followed by corrections to the initial alignment, (iv) generation of dense point cloud and error estimation and (v) production of additional outputs. To analyse and compare the point clouds, the open-source software CloudCompare 2.12.4 was used, allowing to quantify the extent of changes that have occurred in an area. To assess the errors associated with the point clouds, the guidelines proposed by James et al. (2019) have been adopted to describe the accuracy and precision of the survey. In addition, a split data test was performed, as described by the same authors, which involves comparing two areas (plots) assumed to be stable in order to quantify the errors.

3.3 | Multispectral analysis of high-resolution satellite data and DSAS application

The cliff has been investigated considering the high-resolution optical satellite imagery acquired by RapidEye and Planet Scope missions. RapidEye was a constellation of five identical satellites launched in August 2009 and deactivated in March 2020, with a spatial resolution of 5 m and a temporal resolution of 5.5 days (Planet Labs PBC, 2023). Planet Scope is a constellation of over 400 cubesats, launched at various times since June 2016. With a spatial resolution of 3 m and circling Earth every 90 minutes, PlanetScope data are suitable for monitoring rapid changes and mapping (Planet Labs PBC, 2023), especially in coastal areas (Cassidy et al., 2024; Darwish & Smith, 2021). In order to reconstruct the cliff retreat in the years before the field and UAV surveys, we have selected four acquisitions from 2009 to 2021, summarised in the following Table 2.

The satellite-derived cliff crests (SDCCs) in 2009, 2012, 2018 and 2021 are extracted from the limit between vegetation and bare soil computing NDVI (Normalized Difference of Vegetation Index). The perennial vegetation along the cliff edge provides a consistent and reliable marker for delineating the scarp line. Considering the threshold of 0.50, we have extracted four vector representations of the vegetation-bare soil limit (DaSilva et al., 2024).

The Digital Shoreline Analysis System (DSAS) of Himmelstoss et al. (2024) has been widely adopted for computing cliff retreat rates (e.g., Brooks & Spencer, 2010; Brooks, Spencer, & Boreham, 2012; Fullin et al., 2023; Leisner et al., 2023). Using the latest standalone version (DSAS v.6.0.170), it was configured to cast transects at 10 m alongshore spacing, considering the road SP601 as baseline (Figure 3). Since the shoreline, as well as the cliff crest, are naturally influenced by several factors, we have considered the formula proposed by Nassar et al. (2019) for computing the uncertainty of SDCCs:

$$U = \pm\sqrt{Eg^2 + Ep^2 + Ed^2 + Esl^2}$$

The errors due to digitalization (Ed) and sea level fluctuations (Esl) proposed by Nassar et al. (2019) are not considered because i) the cliff crests are automatically extracted, and ii) local sea level fluctuations due to tides do not affect the cliff top. However, we account for errors due to georeferencing (Eg) and pixel size (Ep). For georeferencing, we have evaluated an RMSE of 1.19 and 0.58 m for RE and PS, respectively, while pixel size errors are 5 and for RE and 3 m for PS.

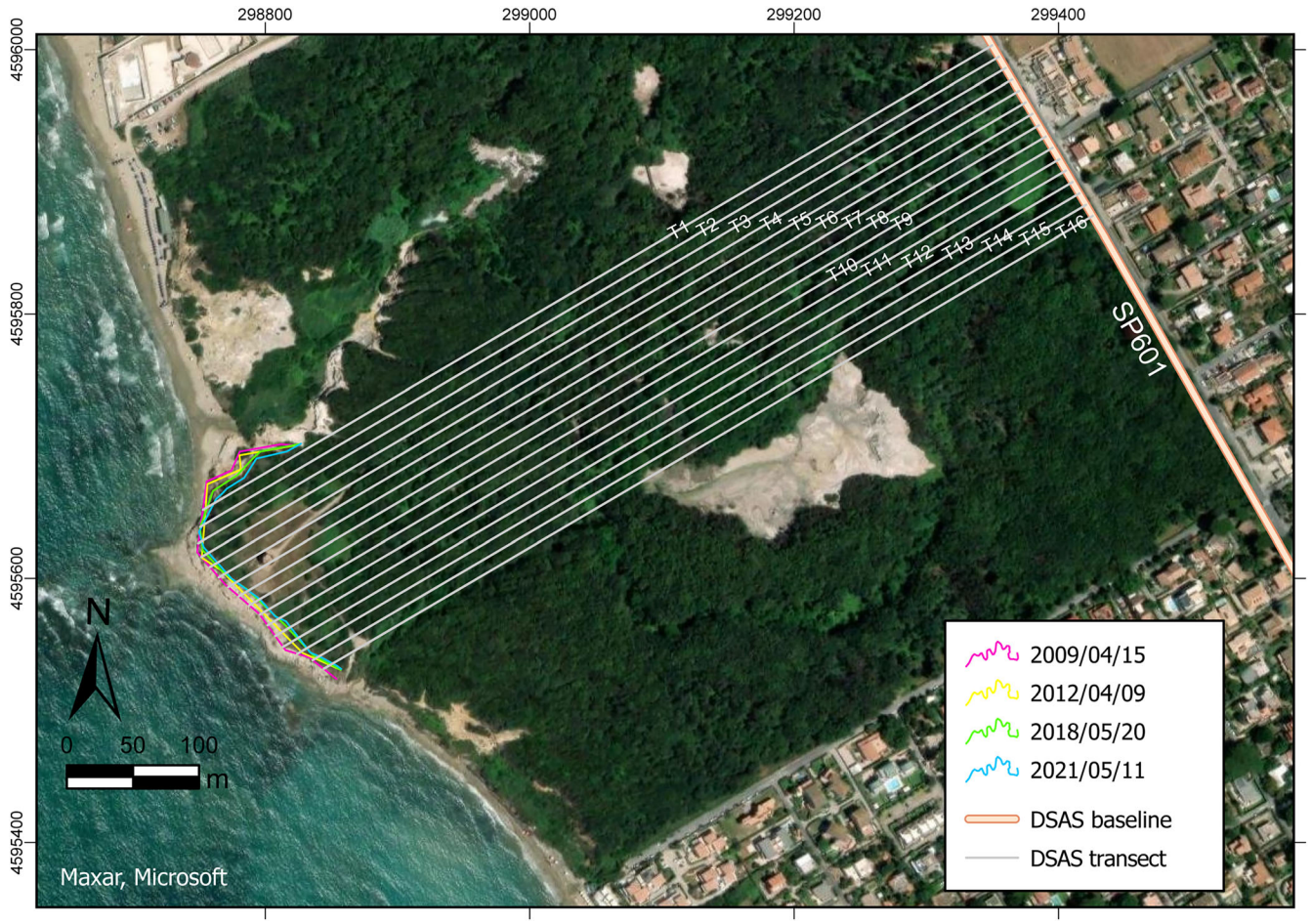

FIGURE 3 The transects (T1-T16) considered in DSAS and the cliff crests reconstructed for 2009, 2012, 2018 and 2009.

The variation in the position of the SDCCs over a specific period is calculated along the transects T1-T16. Considering the SP 601 road as a baseline, we have computed the following statistical metrics: Shoreline Change Rate (SCR), Net Shoreline Movement (NSM), End Point Rate (EPR), Linear Regression Rate (LRR) and Weighted Linear Regression (WLR). Since we are considering the retreat of a cliff, we have modified two indices as follows: SCE has been named as Cliff Change Envelope (CCE), while NSM has been renamed Net Cliff Movement (NCM). Despite Brooks & Spencer (2010) highlights the proneness of LRR to be affected by outliers, several studies have recently demonstrated its applicability in cliff retreat estimations (Castedo et al., 2017; Façanha et al., 2025; Leisner et al., 2023).

3.4 | Marine and meteorological datasets

The marine data of the wave-height were retrieved from the National Wave Buoy Network (RON) and the historical archive of 3BMeteo, both accessible online respectively at the Istituto Superiore per la Protezione e la Ricerca Ambientale website (ISPRA, 2024), and by data request from the 3BMeteo website (3BMeteo, 2024). The data were sampled at a frequency of every 30 minutes for the first dataset, from the Ponza buoy (40°52′00“ N, 12°57′00” E), and every 1 hour for the second dataset, collected off the coast of Anzio. The RON data are collected using a wave sensor placed on the reference buoy. The 3BMeteo data originate from satellite data and point data from buoys and ships; subsequently, these data are processed through numerical forecasting models coupled with atmospheric models to estimate wave heights for the desired location. The two temporal series were then aggregated and analysed using the open-source RStudio 4.3.1 software. First, a correlation analysis was conducted between the two wave height datasets to verify their consistency. The dataset with the most continuous data was used for the subsequent analyses. As a second step, with a Peaks Over Threshold (POT) analysis, which involves identifying the peaks of a time series that exceed a specific threshold (Goda, Kudaka, & Kawai, 2010; Méndez et al., 2006). In our case, the peaks correspond to independent storm events that exceed the chosen threshold. In addition to analysing marine forcings, we evaluated the impact of subaerial processes on slope stability. Specifically, we examined the complementary effects of precipitation, which can directly trigger cliff instability or indirectly contribute to it through physical and chemical weathering (Prémaillon et al., 2018). The rainfall dataset used in this study was freely obtained from the 3BMeteo website (3BMeteo, 2024) for the Anzio locality and it includes daily rainfall for the 2019–2024 period.

4 | RESULTS

Field investigations provided a first detailed geomorphological map of the Tor Caldara coastal area (Figure 4), where landforms are grouped according to their genesis, development, evolution and present

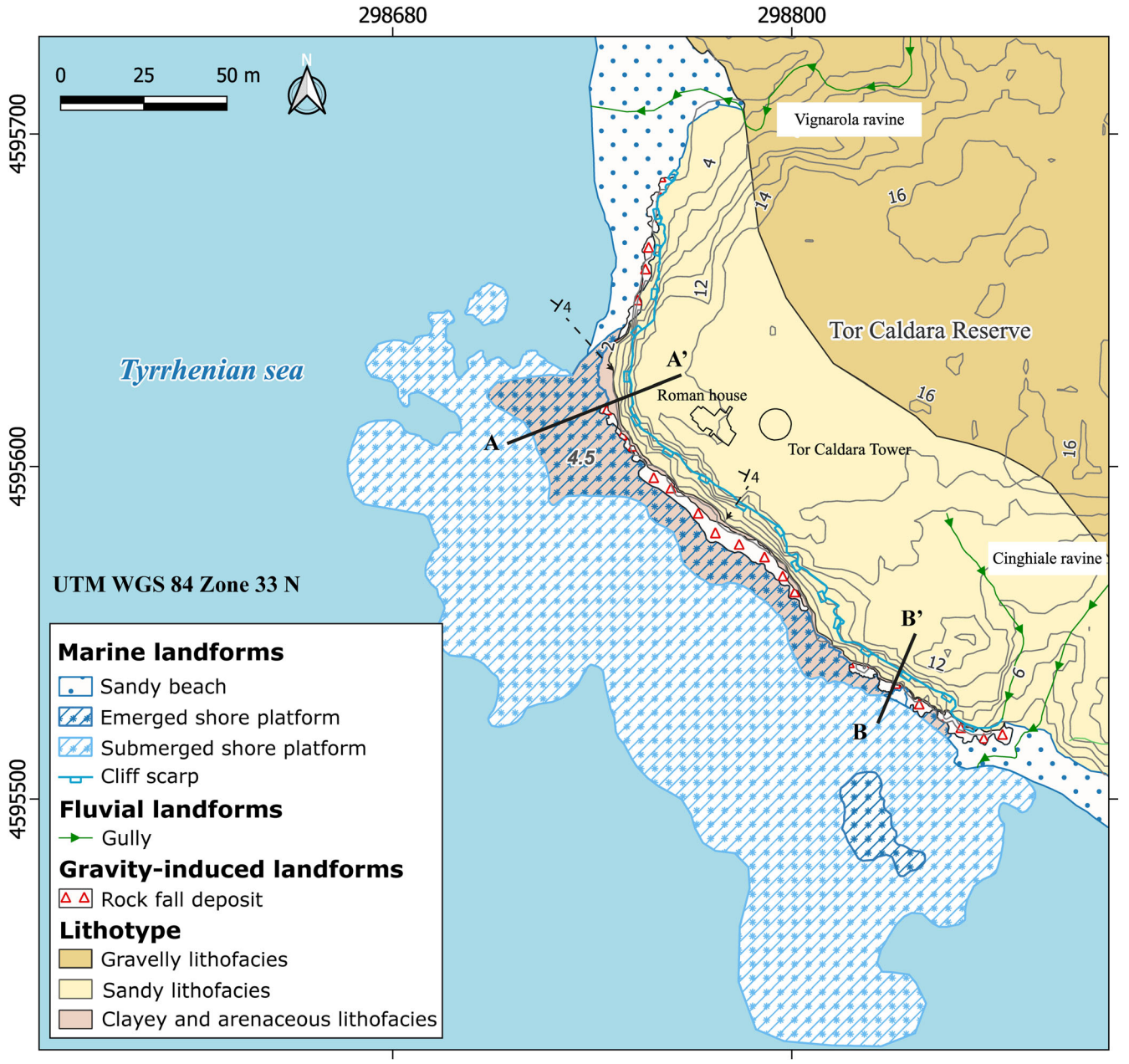

FIGURE 4 Geomorphological map of the tor Caldara coastal area, with the mapping of the submerged shore platform extent and other landforms. The average slope of the emerged shore platform equal to 4.5° is also indicated. The lithology is modified from (Geoportale Regione Lazio, 2024).

dynamics, following the Italian Geomorphological Mapping guidelines (Campobasso et al., 2018). The map is essential for inventorying erosional and depositional landforms, their locations and spatial patterns, which are fundamental to unravel present dynamics and the evolution of the coastal system. The morphology of the Tor Caldara coastal sector can be ascribed to the Type A rocky coast typology proposed by Sunamura (2015), which consists of a gently slopes shore platform, dipping about 4.5°, located at the foot of a sub-vertical cliff. The cliff is classified also as active, according to the Emery & Kuhn (1982) classification both due to the wave action impacting the cliff and the presence of gravity-driven deposits. Most of the shore platform is submerged but, at the tip of the promontory, an emergent section occurs with an extension of approximately 2,500 m^2. The submerged shore platform was mapped using historical optical satellite and recent drone imagery under conditions of extremely calm sea, low tide and clear water. At the base of the cliff, along its entire length, there is also a zone of blocks forming a rock fall deposit. At the N and S of the promontory, near the Vignarola and Cinghiale ravines, predominantly sandy beaches occur.

4.1 | UAV photogrammetric flights and multi-temporal analysis

The study area was subjected to five optical photogrammetric surveys over one year, excluding the summer period due to the higher presence of people on the beach. The UAV surveys were conducted following some storm events or in conjunction with other analyses. Storm events were reviewed using meteo-climatic forecasts, as well as newspapers reporting on storm surges that affected the Anzio area.

TABLE 3 Description of the surveys carried out over one year with the UAV model used and the principal outputs.

Name of the flight	Date (Y-m-d)	UAV model	Number of photos	Number of points
Flight 0 (F0)	2023-05-31	Mavic 2 Pro	690	$\sim 24 \times 10^7$
Flight 1 (F1)	2023-11-10	Mavic 2 Pro	195	$\sim 12 \times 10^7$
Flight 2 (F2)	2024-03-08	Mavic 3 Enterprise	594	$\sim 30 \times 10^7$
Flight 3 (F3)	2024-04-12	Mavic 3 Enterprise	424	$\sim 21 \times 10^7$
Flight 4 (F4)	2024-05-16	Mavic 3 Enterprise	685	$\sim 30 \times 10^7$

For convenience, the photogrammetric surveys will be numbered as in the following Table 3:

Data collected in the five UAV surveys were analysed and compared to each other to identify changes in the landforms. The first multi-temporal analysis was conducted with a visual comparison of the orthophoto-mosaics from each survey. Starting from the F1, rock falls of new blocks from the cliff and the displacement of blocks already present on the beach or shore platform can be observed. The rock fall blocks vary in size from centimetres to metres.

The surveys of 2023 (Figure 5a) were performed with the Mavic 2 Pro, and to obtain a centimetre-level accuracy of the results, six GCPs were distributed throughout the study area. F0 was conducted under conditions of low tide, no wind and clear sky. This survey is considered the base flight upon which all subsequent analyses will be based. The result of F1 highlights the displacement of sandy and pebbly materials on the beach, as well as local metric collapses like those recorded in the northern area near the Vignarola ravine (Figure 5b, c). This survey was conducted during high tide with meter-high waves, where the sea directly impacted the base of the cliff both to the N and S of the emerged shore platform. From the first survey of 2024 (F2), the Mavic 3 Enterprise RTK was employed, partially eliminating the need for GCPs. Between F1 and F2, significant changes occurred both on the cliff and the beach, and rock fallen blocks were found shifted, fractured, or, in some cases, shattered. The most notable differences, however, are observed in the southern part of the rocky coast, just before the Cinghiale ravine (Figure 5d, e). Here, collapses occurred with local cliff retreat, in the mid-slope, of over a metre, clearly visible in the optical images. In the remaining two months (F3 and F4 surveys), rock falls of less than one metre were consistently observed along the entire cliff, with relatively lower intensity compared to the previous events (Figure 5f, g).

In addition to the various rock falls occurring on the cliff, an expansion of some large fractures on the shore platform has been recorded, which generate large blocks separated from the shore platform. Over one year of surveys, comparing the orthophoto-mosaics from F0 to F4, a seaward movement of these large blocks up to approximately 17 cm has been observed (Figure 6). Considering the total errors in the orthophotos from the two surveys (the first conducted using the RS2 + station and the second with the drone RTK sensor, Table 1), which account for errors along the three spatial directions, a maximum uncertainty of ± 8 cm can be added to the previous values of displacement.

4.2 | Point cloud differences

To quantify the changes visible in the optical images, we compared the point clouds from the initial (F0) and final (F4) surveys using the open-source software CloudCompare (Figure 7a). The two-point clouds were cleaned of noise and any outliers, and subsequently, the denser point cloud (F4), was downsampled for a more accurate comparison with the F0 point cloud. The total number of points in the compared clouds for F0 and F4 were 45×10^6 and 70×10^6, respectively. Both point clouds were georeferenced in WGS 84 UTM Zone 33 N. The Point Cloud Difference (PCD) was obtained through the Cloud-to-Cloud Distance (C2C) tool, which calculates the distance between georeferenced points of a reference point cloud and a compared point cloud using various algorithms. In this case, the nearest neighbour distance algorithm was utilized, which searches for the closest point in the reference cloud from a point in the compared cloud and calculates the Euclidean distance (Elkhrachy, 2019); this algorithm is reliable for very dense point clouds. The PCD value scale bar presents absolute values along the three dimensions in space and contains only positive values (Figure 7a). Therefore, images of optical surveys were compared to determine whether there is deposition, indicated by positive values, or erosion, with negative values. In the northern part of the study area, the detachment of the cemented sand (Unit 3) wedge is visible through orange-tinted colours, with PCD values of approximately 0.70 m (Figure 7b, c). Fallen blocks, displaying green-tinted colours, lie just below the marine erosion scarp and exhibit maximum PCD values of 0.20 m (Figure 7b, c). The most intense rock falls are present in the southern part (Figure 7d, e), as optically observed in the previous paragraph. Here, in the PCD, the colours tend to be dark red, indicating the significant retreat in the mid-slope of the cliff, with values up to 1.70 m (Figure 7d, e). The fallen blocks, on the other hand, show values of up to 1 m between the point clouds (Figure 7d, e).

The error values obtained (Table 4) provide a crucial reference for assessing the reliability of the morphological analyses in the study area. Specifically, the error derived from the PCD (PCD F0-F4) represents the global uncertainty threshold for interpreting observed morphological changes. The analysis of the Cloud F0 and Cloud F4 values, reflecting point uncertainties for each cloud, suggests high internal precision for both acquisitions. The addition of the two stable areas (PCD Plot 1, 2; visible in Figure 7a), analysed through the split data test, further supports the analysis. In PCD Plot 1, without vegetation, the error is minimal, suggesting high measurement reliability; in contrast, PCD Plot 2, with low vegetation, shows an error increase, even without topographic changes. Overall, morphological variation analyses are reliable for changes exceeding 0.6 m across the entire area, but in non-vegetated sectors, such as the shore platform and cliff area, significant variations can be detected down to thresholds of approximately 10 cm.

4.3 | Litho-structural and geomechanical data

It is extremely important to analyse the lithological and structural properties of the lithologies of a rocky coast, determining also the

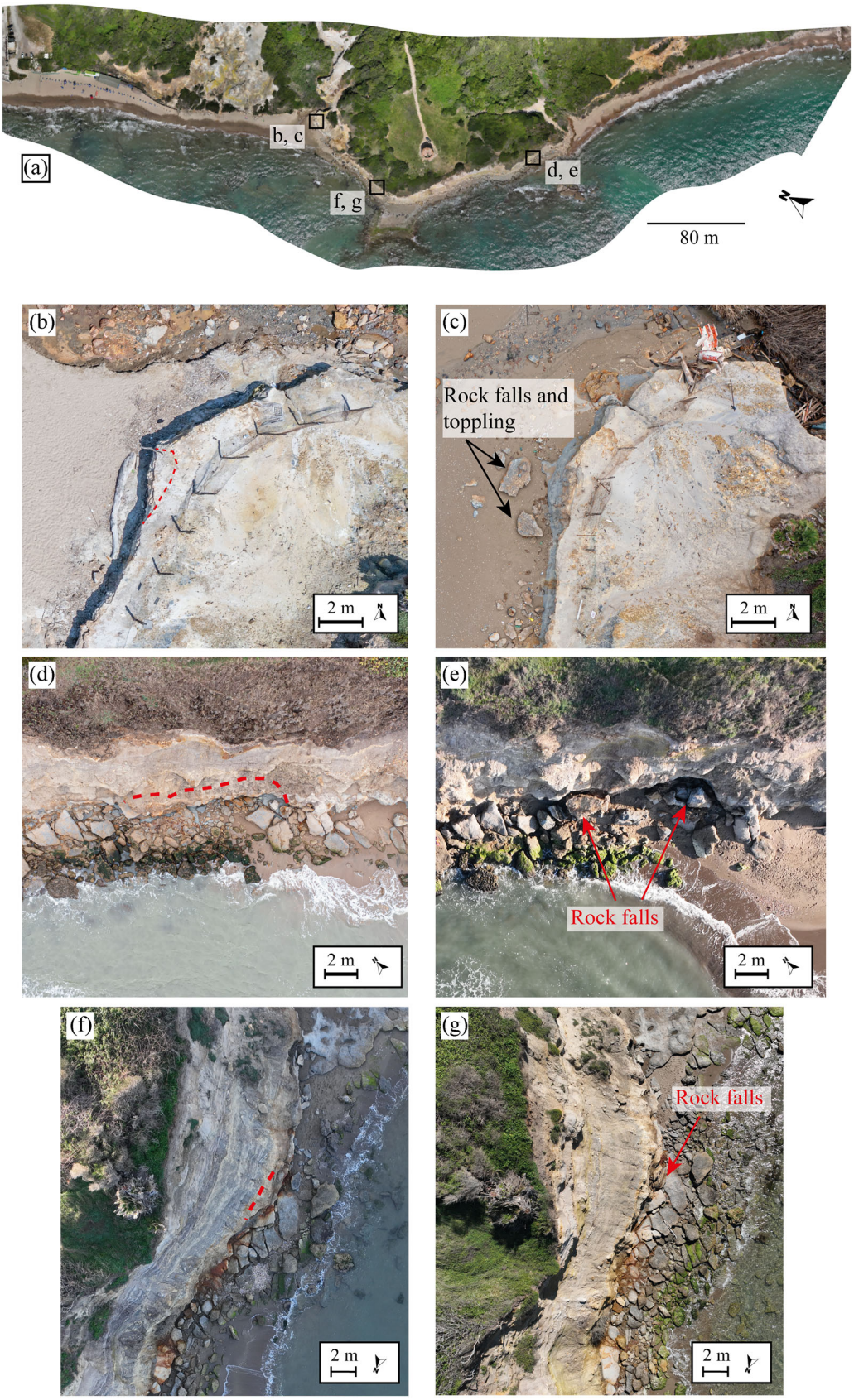

FIGURE 5 Optical multi-temporal analysis of the rocky coastal sector of tor Caldara reserve. a) Orthophoto-mosaic of the tor Caldara study area, one of the first survey outputs (F0) made with Agisoft Metashape software. The other images are captured with UAV surveys and are pre- and post-storm events: F0 (b) vs F1 (c), F1 (d) vs F2 (e) and F2 (f) vs F3 (g), with the red dashed lines and arrows indicating the rock falls.

mechanical strength of the rock mass and joint patterns that control erosion (Budetta, Galietta, & Santo, 2000; Sunamura, 2015). The coastal cliff of Tor Caldara is composed of various lithotypes belonging to different Units, as previously described (Figure 2; 8a, b). In particular, the cliff features two intercalations, part of Unit 1, as highlighted by Bellotti et al. (1997) (Figure 2; 8a, c). The basal

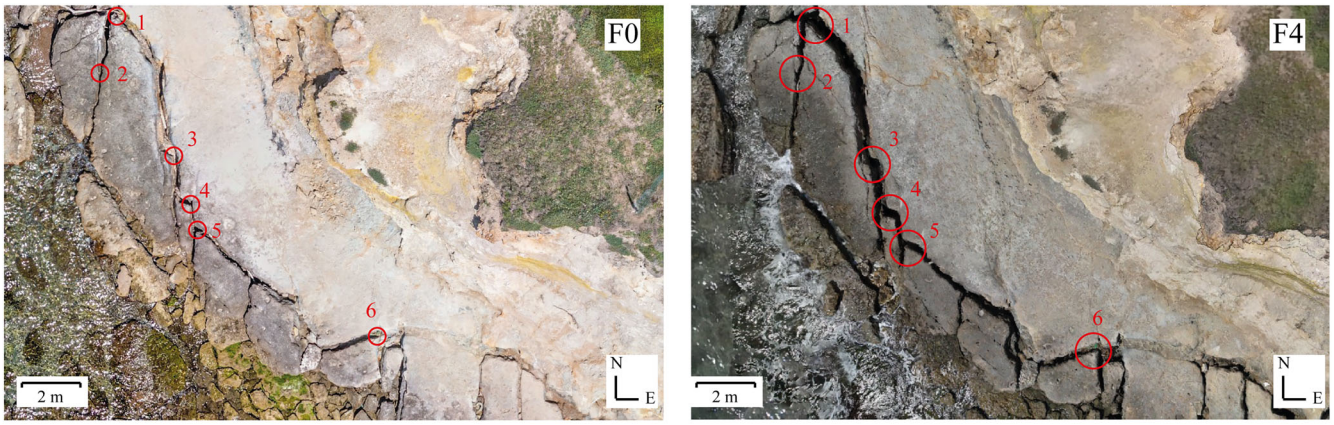

Surveys	1	2	3	4	5	6
F0	37.7 cm	7.57 cm	20.0 cm	25.3 cm	17.1 cm	29.3 cm
F4	52.3 cm	13.8 cm	38.1 cm	34.3 cm	34.5 cm	36.0 cm
Difference	14.6 cm	6.23 cm	18.1 cm	9.0 cm	17.4 cm	6.7 cm

FIGURE 6 Displacement of some large blocks, through the expansion of fractures. The displacement quantification is shown in the table, with the numbers that correspond to the measurement positions.

intercalation is found only in the southernmost part and moving to the N along the coasts, this intercalation disappears beneath the sandstone layer of Unit 3, which forms the shore platform (Figure 8c). Above the shore platform, the second clay intercalation is observed, extending along the entire length of the cliff from the Cinghiale to the Vignarola ravines (Figure 8c) and decreasing in thickness from S to N. The current extent of these two clay layers was identified with the survey F2, after winter storm events eroded much of the thick surface alteration caused by sulphurous risings and percolations that cover the intercalations. The base of the cliff was also subjected to a geomechanical survey aimed at determining the joint pattern and the UCS through the use of a Schmidt Hammer. Due to significant surface weathering of the lithologies, multiple measurements were taken around the specific point of the rock to obtain a representative average of the UCS. For the clay intercalation, UCS values around 33 MPa were recorded, while for the sandstone of Unit 3, the values were approximately 60 MPa; values of the density (KN/m^3) for the clay layers were taken from Bozzano, Martino, & Priori (2006). Unit 3 exhibits three joint families observed across nearly the entire extent of the cliff and represented in the stereoplot included in Figure 8a. The first is the bedding, with a dip direction of about N214°E and a dip angle of 4°; the second fracture system has a dip direction of N261°E and dip angle of 73°, while the third system is oriented at N190°E with a dip of 72°.

4.4 | DSAS application for multitemporal cliff retreat

The computation of NDVI and its classification led to extract four different limits between rock and vegetation, representing the cliff crests during the spring seasons of 2009, 2012, 2018 and 2021. Focusing exclusively on the area encompassing between Vignarola and Cinghiale ravines, we have reconstructed 16 transects (T1-T16), spaced 10 m apart each (Figure 9).

Considering the LRR, along the transects T12 and T13 the cliff shows the highest retreat rates (−1.07 and −1.08 m\yr, respectively), while the transects T2 and T3 at the emerged shore platform present the lowest rates (−0.17 and −0.26 m\yr, respectively). The mean retreat rate is −0.63 m\yr (according to LRR) and slightly decreases to −0.61 m\yr considering the WLR.

Similarly, the maximum distance between the oldest and youngest cliff crests (NCM) is along the transects T12 and T13 (13.39 and 13.79 m, respectively), meanwhile T2 and T3 show the lowest distances (2.65 and 3.61 m, respectively). The same values are confirmed by the CCE, since we are observing the retreat of a cliff and the maximum distance between two cliff crests corresponds to the distance between the oldest and the youngest cliff crests.

The change metrics computed by DSAS are summarised in the following Table 5:

4.5 | Meteorological and marine data

The meteorological and marine data are displayed in Figure 10, which also includes the dates of the various surveys (F0-F4). The downloaded data consist of wave height measurements over the time period from 2019-11-25 to 2024-07-31, with the most recent and continuous time interval of the RON data considered. Since the wave data from the Ponza Network buoy of the RON ended on 2023-11-22, due to a network update, data from 3BMeteo website (3BMeteo, 2024) for the Anzio coast has been also used, overlapping with the previous dataset by approximately 4 years (Figure 10a). The correlation between the two-time series shows a R^2 coefficient of about 0.88 and a p-value of $2.2e^{-16}$ (Figure 10b). With these results, it was therefore decided to continue the subsequent analyses only on the time series provided by 3BMeteo, due to its longer temporal coverage, which spans the entire interval of the surveys. Rainfall data were also downloaded from 3BMeteo website due to their greater temporal continuity over the same time interval as the wave height

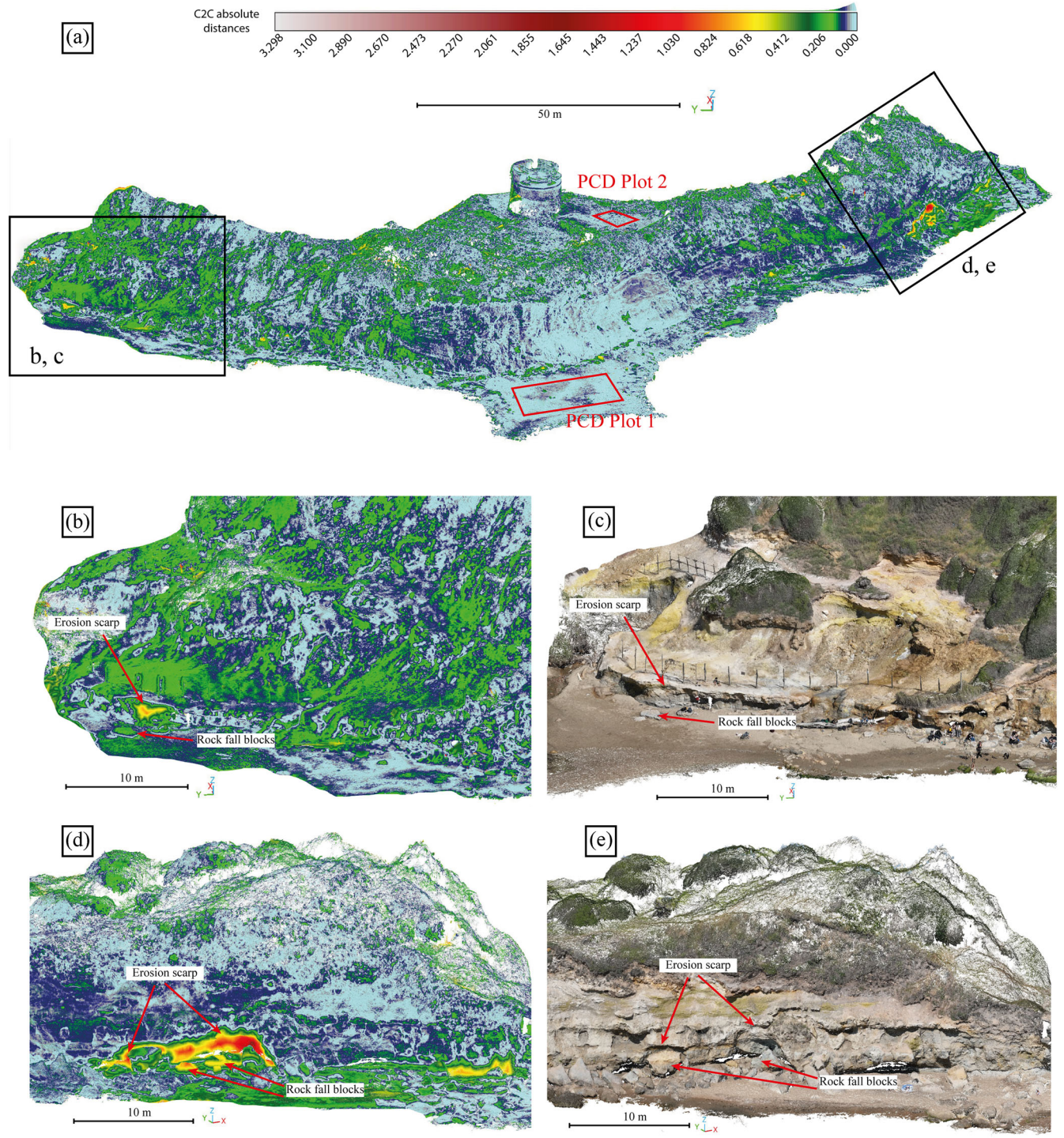

FIGURE 7 Representation of the PCD, showing the metric distances, in the scalar field, between the F0 and F4 point clouds (a). The values of the C2C are expressed in absolute distances and thus only have positive values. For each zoom of the PCD, the image of the optical point cloud is juxtaposed (b-e) to verify whether a specific value corresponds to the deposition or erosion of material.

data. The graph (Figure 10c) shows a general decrease in both the intensity and duration of rainfall events from summer 2023 to July 2024.

To identify wave peaks that could potentially coincide with a storm event, the POT analysis was conducted (Figure 10), choosing the threshold as the third standard deviation, with a value of 2.44 m, corresponding to the 98th percentile. To calculate the time required for an event to be considered independent, an autocorrelation analysis was performed, revealing that for the given data, two peaks of probable storm events are independent if more than 48 hours have passed with heights below the threshold. The results indicate that while the number of storm events has not significantly changed over the analysed years, there is an observed local increase in the intensity of winter storms (November–December) and the occurrence of exceptional off-season events, such as the peaks in July and August 2023, with wave height reaching up to 4 m.

5 | DISCUSSION

5.1 | Evolution of the rocky coast

As evident from the results of this study, the rocky coast of Tor Caldara exhibits signs of pronounced morphological changes within just one year of monitoring. The cliff face exhibits a complex pattern of erosion and deposition, with the southern section demonstrating locally up to 1 m of retreat (Figure 7a, d). Similarly, DSAS analysis on 2009, 2012, 2018 and 2021 SDCCs indicates a mean retreat rate of approximately 0.6 m\yr (based on LRR and WLR) along the cliff between Vignarola and Cinghiale ravines. Notably, the highest LRR, around 1.0 m\yr along transects T12 and T13, aligns with the maximum retreat rate observed in the southern cliff sector (Figure 9).

The observed morphoevolution is characterized by a combination of gradual and paroxysmal changes. Gradual processes include continuous weathering and mass wasting along the cliff face, characterized by the smaller-scale rock falls. These ongoing events contribute to the overall retreat of the coastline and the reshaping of the cliff profile. More dramatic morphological changes were observed in the form of larger mass movements, especially in the southern section of the cliff (Figure 5; 7). In this region, we recorded substantial cliff retreats, with some areas experiencing recession of up to 1.70 m in the mid-slope area. These events led to significant alterations in the cliff face geometry, creating new erosional surfaces and depositing substantial amounts of material at the cliff base that not only modify the local topography but also influence the dynamics of wave-cliff interactions, potentially accelerating future erosion processes. Moreover, the spatial variability in erosion intensity along the cliff face suggests a complex interplay of drivers influencing coastal evolution.

TABLE 4 Summary of the errors in the validation of F0 and F4 photogrammetric surveys. ME = mean error; MAE = mean absolute error; SDE = standard deviation error; RMSE = root mean square error.

	ME	MAE	SDE	RMSE
Cloud F0	0.0343	0.0343	0.0703	0.0782
Cloud F4	0.0344	0.0344	0.1307	0.1351
PCD (F0-F4)	0.0092	0.1956	0.5983	0.5983
PCD Plot 1	−0.0211	0.0328	0.0990	0.1012
PCD Plot 2	−0.0105	0.0647	0.1875	0.1877

5.2 | Analysis of the drivers controlling morphoevolution

Over the years many studies have attempted to identify and comprehend the drivers that influence the evolution of a rocky coast (Brooks,

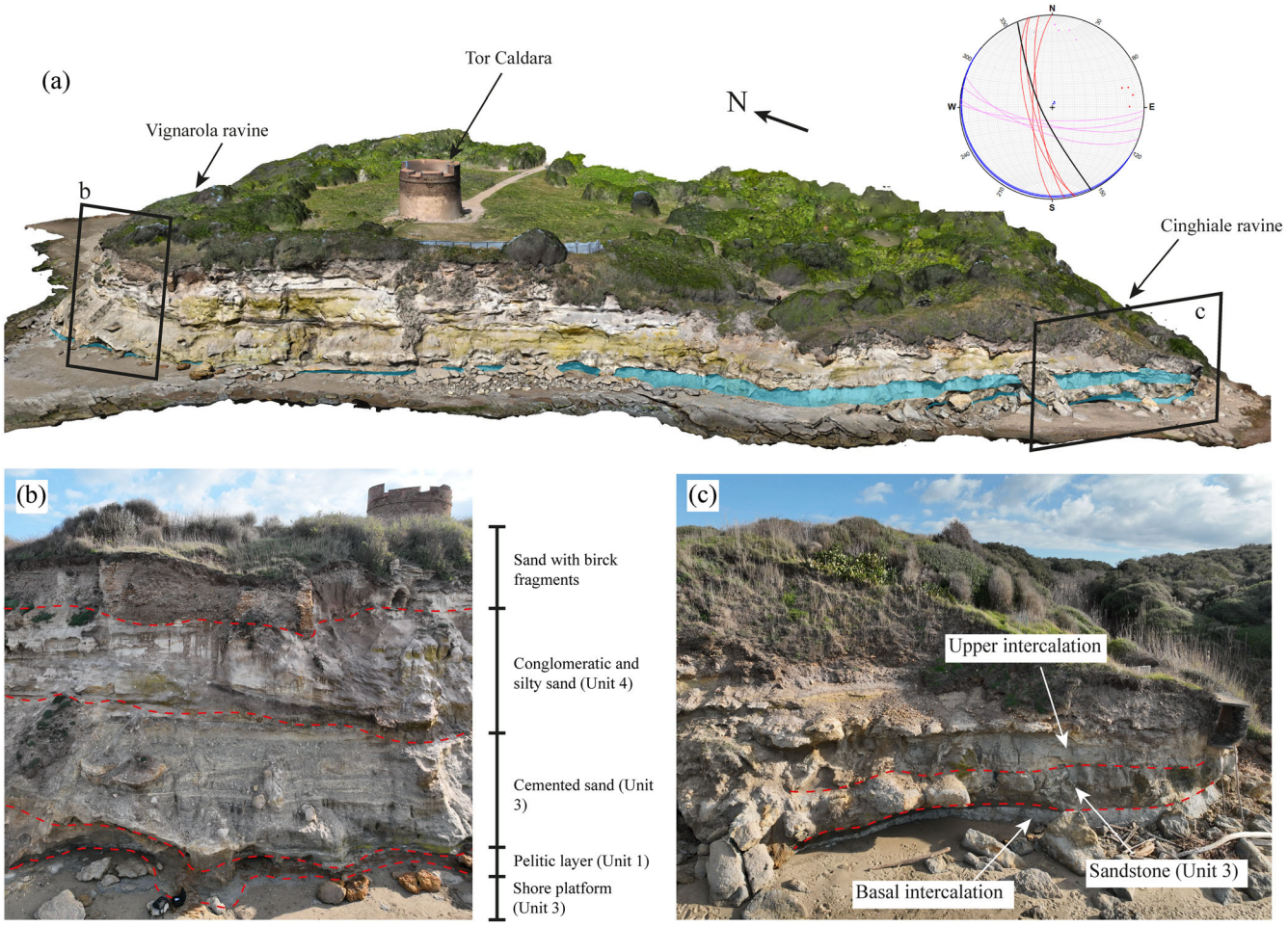

FIGURE 8 Extent of the two clay layers (light blue polygons), with greater thickness in the southern part of the study area (a); a stereoplot with the main joint families common in the total extent of the cliff is also visible. The stratigraphy of the cliff with the different units is visible in zoom b). In the southern part, the two clay intercalations can be clearly seen terminating at the Cinghiale ravine c).

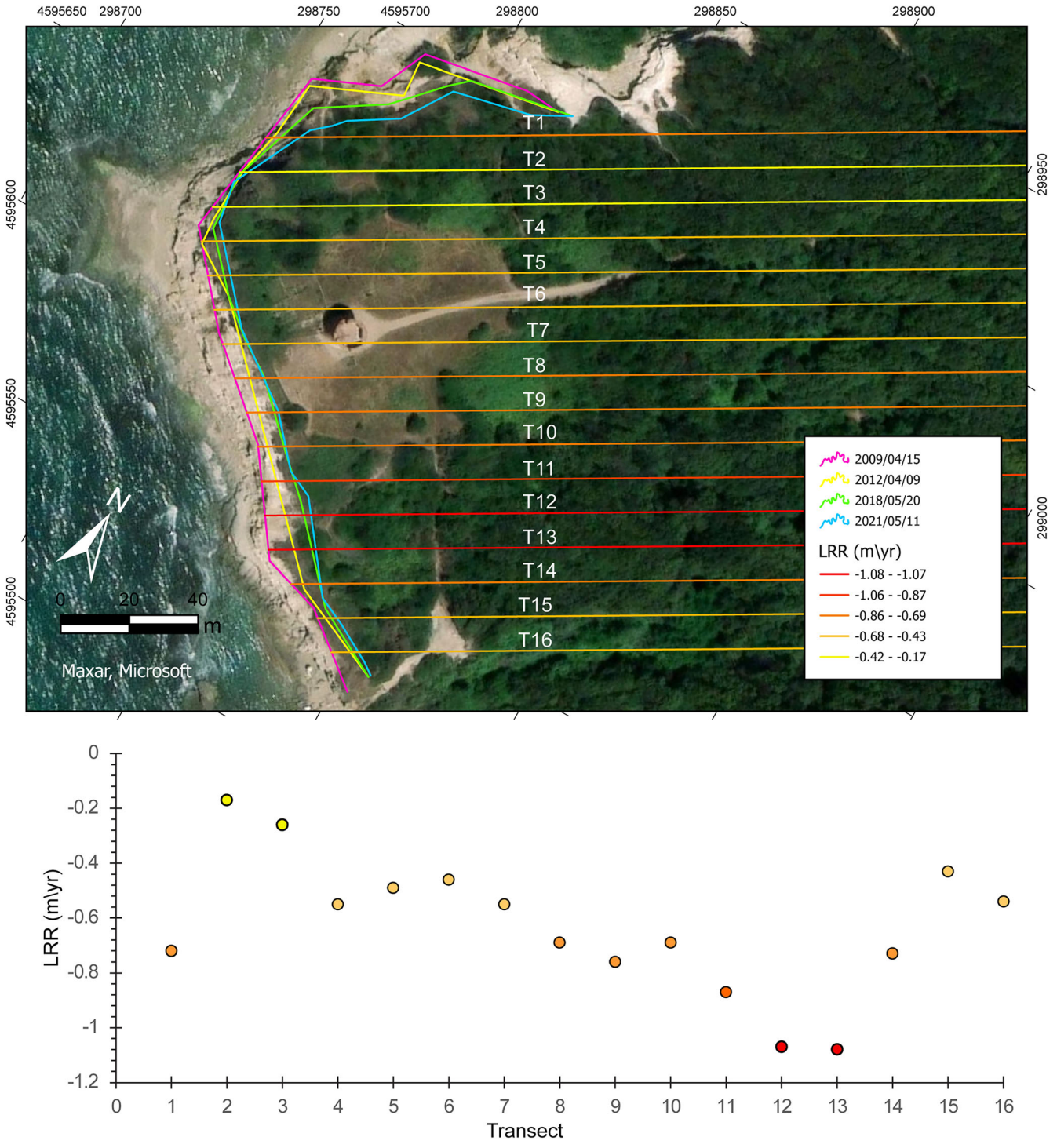

FIGURE 9 The DSAS transects coloured according to the linear regression rate (LRR). The basemap is the optical satellite imagery available in ArcGIS pro 3.4.0, derived from Maxar's satellites collecting the highest resolution satellite imagery commercially available (0.15 and 0.30 m).

Spencer, & Boreham, 2012; Fullin et al., 2024; Hurst et al., 2016; Limber et al., 2018; Prémaillon et al., 2018; Troiani et al., 2020). In this work, these drivers have been categorized into three groups, as previously proposed by Prémaillon et al. (2018). These categories include: (i) continental forcing, such as rainfall or frost; (ii) marine forcing, primarily due to the action of the sea; (iii) cliff setting, which encompasses morphological, structural and lithological characteristics.

Regarding the analysed rainfall time interval (Figure 10c), no exceptional or prolonged events were recorded, during the 2023–2024 period. On the contrary, the rainfall trend for this period shows a marked decrease compared to the previous interval, which was characterized by higher precipitation and rainfall peaks of up to 70 mm. It is plausible to assume that, for our study area, the impact of precipitation is limited compared to other forcing drivers, as there is an observed increase in mass wasting processes despite the reduced rainfall intensity compared to the previous years. Rainfall likely plays a role more related to preparing the rock mass for collapse events by gradually weakening it (Prémaillon et al., 2018), rather than acting as an immediate trigger. However, due to the lack of mass wasting data for the previous interval, we cannot exclude the possibility that rainfall also had a significant role as a trigger for localized rock-block and debris detachments.

TABLE 5 The change metrics computed for each transect: CCE (cliff change envelope), NCM (net change movement), EPR (end point rate), LRR (linear regression rate), WLR (weighted linear regression).

Transect id	CCE (m)	NCM (m)	EPR (m\yr)	LRR (m\yr)	WLR (m\yr)
T1	9.78	9.78	−0.81	−0.72	−0.77
T2	2.65	2.65	−0.22	−0.17	−0.19
T3	3.61	3.61	−0.3	−0.26	−0.25
T4	6.34	6.34	−0.53	−0.55	−0.56
T5	6.53	6.53	−0.54	−0.49	−0.49
T6	6.72	6.72	−0.56	−0.46	−0.44
T7	7.42	7.42	−0.61	−0.55	−0.51
T8	8.63	8.63	−0.69	−0.69	−0.65
T9	9.22	9.22	−0.76	−0.76	−0.74
T10	7.98	7.98	−0.66	−0.69	−0.66
T11	10.48	10.48	−0.87	−0.87	−0.83
T12	13.39	13.39	−1.11	−1.07	−1.04
T13	13.79	13.79	−1.14	−1.08	−1.03
T14	8.55	8.55	−0.71	−0.73	−0.69
T15	5.57	5.57	−0.46	−0.43	−0.43
T16	7.83	7.83	−0.65	−0.54	−0.52

The statistical analysis of the time series data reveals a strong correlation between wave height measurements from the RON and the 3BMeteo dataset. This consistency is crucial as it validates the accuracy of the 3BMeteo data, providing confidence in using this information to fill gaps or extend the temporal coverage of the wave height time series analysis, particularly when the RON buoy measurements might be sparse or non-existent. As shown in Figure 10b, the correlation plot displays an almost perfect linear relationship between the two datasets, indicating they are capturing the same wave height dynamics. However, the gradient of the correlation curve is shifted towards the 3BMeteo axis, suggesting this dataset tends to report lower wave height values compared to the RON buoy network. This discrepancy can likely be explained by the different geographic locations of the measurement sources. The RON buoy is located further offshore and may be exposed to wave conditions of greater intensity compared to the 3BMeteo instruments situated closer to the coast near Anzio.

The analysis of the 3BMeteo time series data (Figure 10a) also provided valuable insights into the temporal patterns of wave height extremes in the study region. By identifying significant wave height peaks exceeding 2.44 m within 48-hour intervals, we were able to isolate distinct event peak occurrences within the investigated timeframe. The analysis revealed a recurring seasonal trend, with frequent storm events predominantly occurring during the winter and spring periods, consistent with the climatic asset of the coast (Fortelli et al., 2021; Littmann, 2000), typically from December through April–May of each year (Figure 10a). The similarity in the intensity and frequency of these seasonal storm events suggests a consistent regional wave climate, with some spots of significant variations observed for example in the summer of 2023 and in the magnitude of the autumn-winter of 2023 (Figure 10a). Although there are some high-intensity events (up to 4 m in wave height), the overall pattern of data, including the number of seasonal and annual storm events, remains relatively consistent. Given the general absence of significant variations in marine drivers, we presume that their role is more preparatory than triggering, impacting on the rock mass resistance and contributes to undercutting at the base, rather than causing detachments during wave impacts.

The last driver to consider is the cliff setting. The role of the clay intercalations (Figure 2; 8a) at the base of the cliff and beneath the shore platform is crucial. These intercalations are eroded by the sea, predisposing the overlying Unit 3 to rock falls. At this point, the condition of the rock mass becomes significant, as the two joint families detach the block from the cliff, which eventually collapses once the support provided by the clays is removed. The two discontinuity systems are also clearly recognizable in the shore platform (Figure 5, and stereoplot in Figure 8), which exhibits a different style of evolution. Here, the blocks appear to slowly slide along the submerged intercalation beneath the platform towards the sea, evidenced by the widening of fractures that already separate the blocks from the original shore platform.

Sulphur upwellings also can play an important role. Most of the surfaces of the cliff and the fillings of the discontinuities, both in the platform and in the cliff, are affected by sulphur precipitation. Sulphur can ascend through fractures, precipitating and gradually widening them. In this preliminary study, however, this additional characteristic was not considered, with the focus primarily on the driving forces that play a fundamental role across the majority of rocky coasts.

Consequently, the outcropping lithologies and the structural conditions of the rock mass play a fundamental role in the evolution of the Tor Caldara rocky coasts. However, it's important to note that drone monitoring is discontinuous and does not allow for recording the actual wave impact on the cliff. To evaluate the potential triggering action of wave motion in relation to recorded rock falls, a real-time video monitoring system and other different sensors would be necessary. This would enable data acquisition in any weather condition and, crucially, record the exact timing of rock detachments from the cliff face.

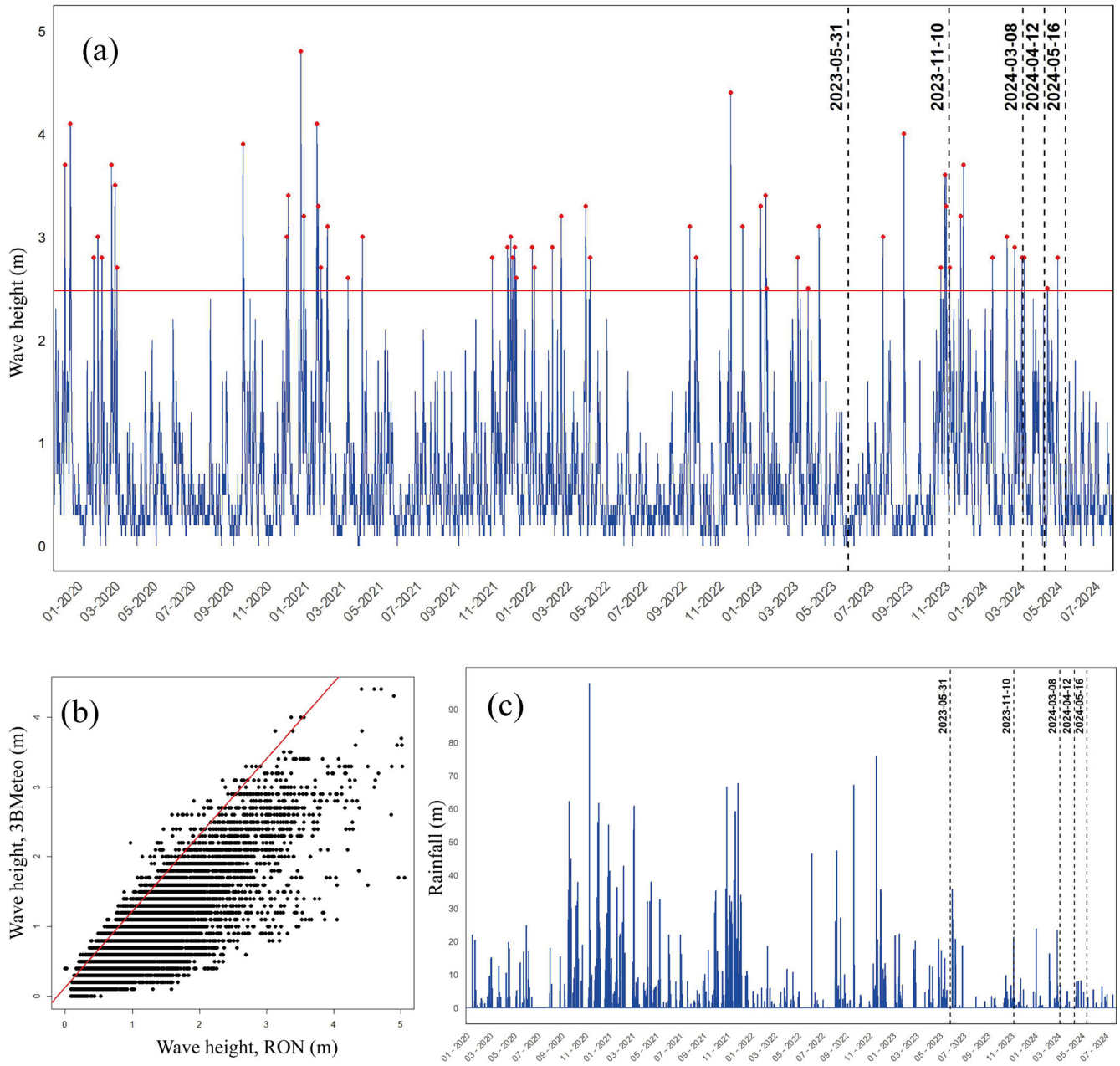

FIGURE 10 POT analysis on the 3BMeteo (3BMeteo, 2024) wave height dataset for the period from 2019 to 11-25 to 2024-07-31, showing the number of events over the threshold (a) (see the text for details); correlation between the RON and 3BMeteo wave height datasets show an highest R^2 coefficient of about 0.88 (b); rainfall data from 3Bmeteo (3BMeteo, 2024) for the same 2019–2024 period, displaying the general decrease in intensity and duration of the events (c).

6 | CONCLUSIONS

This study provides an analysis of the drivers influencing the evolution of the soft rocky coast at Tor Caldara Nature Reserve, utilizing an integrated approach that combines traditional field surveys, UAV campaigns and high-resolution satellite imagery analysis. The development of a detailed geomorphological map through field surveys has highlighted the current distribution of erosional and depositional landforms along the coastal sector, providing a crucial baseline for future monitoring efforts. Moreover, these surveys enabled a thorough characterization of the litho-structural properties of the outcropping rocks, which proved to be a fundamental driver in understanding the evolutionary processes of the coast. The application of repeated UAV surveys, coupled with point cloud comparison techniques, allowed for precise quantification of cliff collapses and detailed observation of morphological changes over time. This high-resolution temporal and spatial data has revealed a pattern of both gradual and paroxysmal changes, with the southern section of the study area experiencing the most pronounced morphological alterations, including cliff retreats of up to 1.70 m in the mid-slope area. Furthermore, the SDCCs from 2009, 2012, 2018 and 2021 analysed using DSAS, provide valuable additional data for a more comprehensive understanding of the cliff's morphodynamics over time.

Through a systematic analysis of marine (e.g., wave action), continental (i.e., rainfall) and morphological drivers (i.e., cliff morphology and litho-structural characteristics) on coastal evolution, we have identified several key outcomes for our study area:

1. Marine drivers: while wave action, particularly during storm events, plays a crucial role in erosion processes, our data suggest that its impact is more preparatory than triggering. The consistent pattern of seasonal storm events, predominantly occurring from December through April–May, contributes to the long-term weakening of the cliff structure.
2. Continental drivers: contrary to initial expectations, rainfall appears to have a limited direct impact on erosion events in our study area. The observed increase in cliff rockfalls and erosion despite reduced rainfall intensity suggests that precipitation likely plays a more indirect role in gradually weakening the rock mass.
3. Morphological drivers: The litho-technical features of the cliff, including the presence of clay intercalations at the base and the two prominent joint families, emerge as the most critical drivers in determining the cliff evolution. The erosion of clay layers by wave action predisposes the overlying units to rock falls, while the joint systems facilitate block detachment once support is removed.

This study confirms the effectiveness of combining field and UAV surveys to determine the key drivers shaping the evolution of a rocky coast. The research conducted at Tor Caldara Nature Reserve has broader implications for coastal management and risk mitigation strategies, particularly in areas of significant natural and cultural heritage. By identifying the primary drivers of coastal evolution, this study lays the foundation for more targeted and effective conservation efforts. However, to fully develop robust management strategies, future monitoring efforts should integrate multiple sensors, including video cameras, seismic sensors, fracture extension sensors and gas emission sensors along fractures. These technologies, combined with optical, LiDAR and multispectral UAV-based surveys, will enhance the quantitative discrimination of the processes driving coastal erosion. Additionally, collaboration with local and regional authorities will be crucial in developing strategic protection measures.

AUTHOR CONTRIBUTIONS

D.T.: conceptualization, methodology; investigation; resources; writing – initial draft; writing – review and editing. **M.Z.:** conceptualization, methodology; investigation; writing – initial draft; writing – review and editing. **G.I.:** conceptualization, methodology, writing – review and editing. **M.M.:** investigation. **R.T.:** investigation. **F.T.:** investigation, supervision, writing – review and editing. **D.P.:** funding acquisition, investigation, supervision, writing – review and editing.

ACKNOWLEDGEMENTS

This study was carried out within the RETURN Extended Partnership and received funding from the European Union Next-GenerationEU (National Recovery and Resilience Plan – NRRP, Mission 4, Component 2, Investment 1.3 – D.D. 1243 2/8/2022, PE0000005).

DATA AVAILABILITY STATEMENT

Wave and rainfall data are available upon request at the 3BMeteo website (https://www.3bmeteo.com/servizi/storico) and at the ISPRA website (https://www.mareografico.it). The LiDAR data are available at the Geoportale MASE website (https://gn.mase.gov.it/portale/home). Other data are available on request from the corresponding author.

CONFLICT OF INTEREST STATEMENT

The authors declare that they have no conflict of interest.

ORCID

Davide Torre https://orcid.org/0000-0001-8880-975X
Marta Zocchi https://orcid.org/0000-0002-8890-0331
Giulia Iacobucci https://orcid.org/0000-0002-1419-1536
Marco Menichetti https://orcid.org/0000-0003-2901-0715
Francesco Troiani https://orcid.org/0000-0002-4554-1332
Daniela Piacentini https://orcid.org/0000-0002-5235-3882

REFERENCES

3BMeteo. (2024). Meteo-marine data archives. Accessed July 31, 2024 https://www.mareografico.it

Aucelli, P.P.C., Di Paola, G., Rizzo, A. & Rosskopf, C.M. (2018) Present day and future scenarios of coastal erosion and flooding processes along the Italian Adriatic coast: the case of Molise region. *Environmental Earth Sciences*, 77(10), 371. Available from: https://doi.org/10.1007/s12665-018-7535-y

Beck, H.E., Zimmermann, N.E., McVicar, T.R., Vergopolan, N., Berg, A. & Wood, E.F. (2018) Present and future Köppen-Geiger climate classification maps at 1-km resolution. *Scientific Data*, 5(1), 180214. Available from: https://doi.org/10.1038/sdata.2018.214

Bellotti, P., E, S., Tortora, P. & Valeri, P. (1997) Caratteri sedimentologici e stratigrafici dei sedimenti Plio-pleistocenici affioranti lungo la costa tra Tor Caldara a Anzio (Lazio Centrale). *Bollettino- Societa Geologica Italiana*, 116, 79–94.

Bozzano, F., Martino, S. & Priori, M. (2006) Natural and man-induced stress evolution of slopes: the Monte Mario hill in Rome. *Environmental Geology*, 50(4), 505–524. Available from: https://doi.org/10.1007/s00254-006-0228-y

Brooks, S.M. & Spencer, T. (2010) Temporal and spatial variations in recession rates and sediment release from soft rock cliffs, Suffolk coast, UK. *Geomorphology*, 124(1–2), 26–41. Available from: https://doi.org/10.1016/j.geomorph.2010.08.005

Brooks, S.M., Spencer, T. & Boreham, S. (2012) Deriving mechanisms and thresholds for cliff retreat in soft-rock cliffs under changing climates: rapidly retreating cliffs of the Suffolk coast, UK. *Geomorphology*, 153, 48–60. Available from: https://doi.org/10.1016/j.geomorph.2012.02.007

Bucci, F., Santangelo, M., Fongo, L., Alvioli, M., Cardinali, M., Melelli, L., et al. (2022) A new digital lithological map of Italy at the 1:100 000 scale for geomechanical modelling. *Earth System Science Data*, 14(9), 4129–4151. Available from: https://doi.org/10.5194/essd-14-4129-2022

Budetta, P., Galietta, G. & Santo, A. (2000) A methodology for the study of the relation between coastal cliff erosion and the mechanical strength of soils and rock masses. *Engineering Geology*, 56(3-4), 243–256. Available from: https://doi.org/10.1016/S0013-7952(99)00089-7

Campobasso, C., Carton, A., Chelli, A., D'Orefice, M., Dramis, F., Graciotti, R., et al. (2018) *Aggiornamento ed Integrazioni Delle Linee Guida Della Carta Geomorfologica d'Italia Alla Scala 1:50.000*. Roma, Italy: Quaderni serie III, ISPRA, Servizio Geologico d'Italia, p. 13.

Carapezza, M.L., Barberi, F., Ranaldi, M., Tarchini, L. & Pagliuca, N.M. (2019) Faulting and gas discharge in the Rome area (Central Italy) and associated hazards. *Tectonics*, 38(3), 941–959. Available from: https://doi.org/10.1029/2018TC005247

Cassidy, G., Wiseman, M., Lange, K., Eilers, C. & Bradley, A. (2024) Seasonal coastal erosion rates calculated from PlanetScope imagery in Arctic Alaska. *Remote Sensing*, 16(13), 2365. Available from: https://doi.org/10.3390/rs16132365

Castedo, R., Paredes, C., de la Vega-Panizo, R. & Santos, A.P. (2017) The modelling of coastal cliffs and future trends. In: Shukla, D. (Ed.) *Hydro-geomorphology-models and trends*. IntechOpen. Available from: https://doi.org/10.5772/intechopen.68445

Cavalli, R.M. (2024) Remote data for mapping and monitoring coastal phenomena and parameters: a systematic review. *Remote Sensing*, 16(3), 446. Available from: https://doi.org/10.3390/rs16030446

Cevasco, A., Pepe, G. & Brandolini, P. (2014) The influences of geological and land use settings on shallow landslides triggered by an intense rainfall event in a coastal terraced environment. *Bulletin of Engineering Geology and the Environment*, 73(3), 859–875. Available from: https://doi.org/10.1007/s10064-013-0544-x

Colantoni, A., Mavrakis, A., Sorgi, T. & Salvati, L. (2015) Towards a 'polycentric' landscape? Reconnecting fragments into an integrated network of coastal forests in Rome. *Rendiconti Lincei*, 26(S3), 615–624. Available from: https://doi.org/10.1007/s12210-015-0394-5

D'Angelo, S., Gisotti, G., Lembo, P. & Valletta, M. (1999) *Rischio geologico della fascia costiera e problematiche di conservazione della spiaggia tra Anzio e Tor Caldara*. La villa di Nerone e la costa di Anzio: Problemi di salvaguardia e studio del porto di Nerone, pp. 29–38.

Darwish, K. & Smith, S. (2021) A comparison of Landsat-8 OLI, Sentinel-2 MSI and PlanetScope satellite imagery for assessing coastline change in El-Alamein, Egypt. *Engineering Proceedings*, 10(1), 23. Available from: https://doi.org/10.3390/ecsa-8-11258

DaSilva, M.D., Hesp, P.A., Bruce, D., Downes, J. & Miot da Silva, G. (2024) Coastal transgressive dunefield evolution as a response to multi-decadal shoreline erosion. *Geomorphology*, 455, 109165. Available from: https://doi.org/10.1016/j.geomorph.2024.109165

Delchiaro, M., Della Seta, M., Martino, S., Moumeni, M., Nozaem, R., Marmoni, G.M., et al. (2024) The role of long-term preparatory factors in mass rock creep deforming slopes: insights from the Zagros Mts. Belt (Iran). *Landslides*, 21(8), 1735–1755. Available from: https://doi.org/10.1007/s10346-024-02252-6

Devoto, S., Macovaz, V., Mantovani, M., Soldati, M. & Furlani, S. (2020) Advantages of using UAV digital photogrammetry in the study of slow-moving coastal landslides. *Remote Sensing*, 12(21), 3566. Available from: https://doi.org/10.3390/rs12213566

Di Bella, L., Carboni, M.G., Bergamin, L. & Iamundo, F. (2005) The Early Pleistocene in Latium (Central Italy): palaeoecology from benthic foraminiferal record. *Quaternary International*, 131(1), 23–34. Available from: https://doi.org/10.1016/j.quaint.2004.07.007

Di Bella, L., Raffi, R., Alivernini, M., Baldassarre, M.A., Barbieri, M., Bellotti, P., et al. (2020) Coastal morphodynamics and environmental assessment of the special protection site of Palude di Torre Flavia (Tyrrhenian Sea, Italy). *Environmental Earth Sciences*, 79(23), 514. Available from: https://doi.org/10.1007/s12665-020-09257-z

Elkhrachy, I. (2019) Modeling and visualization of three dimensional objects using low-cost terrestrial photogrammetry. *International Journal of Architectural Heritage*, 14(10), 1456–1467. Available from: https://doi.org/10.1080/15583058.2019.1613454

Emery, K.O. & Kuhn, G.G. (1982) Sea cliffs: their processes, profiles, and classification. *Geological Society of America Bulletin*, 93(7), 644–654. Available from: https://doi.org/10.1130/0016-7606(1982)93<644:SCTPPA>2.0.CO;2

Esposito, G., Salvini, R., Matano, F., Sacchi, M., Danzi, M., Somma, R., et al. (2017) Multitemporal monitoring of a coastal landslide through SfM-derived point cloud comparison. *The Photogrammetric Record*, 32(160), 459–479. Available from: https://doi.org/10.1111/phor.12218

Façanha, M.C., Albuquerque, M.D.G., de Paula, D.P., Leisner, M., Espinoza, J.M.D.A., Vasconcelos, Y.G., et al. (2025) Medium-term analysis of coastal cliff retreat change at Pacheco Beach, northeastern Brazil. *Journal of Coastal Research*, 113(SI), 335–340. Available from: https://doi.org/10.2112/JCR-SI113-066

Faccenna, C., Funiciello, R., Bruni, A., Mattei, M. & Sagnotti, L. (1994) Evolution of a transfer-related basin: the Ardea basin (Latium, Central Italy). *Basin Research*, 6(1), 35–46. Available from: https://doi.org/10.1111/j.1365-2117.1994.tb00073.x

Fortelli, A., Fedele, A., De Natale, G., Matano, F., Sacchi, M., Troise, C., et al. (2021) Analysis of sea storm events in the Mediterranean Sea: the case study of 28 December 2020 sea storm in the Gulf of Naples, Italy. *Applied Sciences*, 11(23), 11460. Available from: https://doi.org/10.3390/app112311460

Francioni, M., Coggan, J., Eyre, M. & Stead, D. (2018) A combined field/remote sensing approach for characterizing landslide risk in coastal areas. *International Journal of Applied Earth Observation and Geoinformation*, 67, 79–95. Available from: https://doi.org/10.1016/j.jag.2017.12.016

Fratianni, S. & Acquaotta, F. (2017) The Climate of Italy. In: Soldati, M. & Marchetti, M. (Eds.) *Landscapes and landforms of Italy*. Cham: Springer International Publishing, pp. 29–38. Accessed 26, October 2023 http://link.springer.com/10.1007/978-3-319-26194-2_4

Fullin, N., Duo, E., Fabbri, S., Francioni, M., Ghirotti, M. & Ciavola, P. (2023) Quantitative characterization of coastal cliff retreat and landslide processes at Portonovo–Trave cliffs (Conero, Ancona, Italy) using multi-source remote sensing data. *Remote Sensing*, 15(17), 4120. Available from: https://doi.org/10.3390/rs15174120

Fullin, N., Fraccaroli, M., Francioni, M., Fabbri, S., Ballaera, A., Ciavola, P., et al. (2024) Detection of cliff top erosion drivers through machine learning algorithms between Portonovo and Trave cliffs (Ancona, Italy). *Remote Sensing*, 16(14), 2604. Available from: https://doi.org/10.3390/rs16142604

Furlani, S., Bolla, A., Hastewell, L., Mantovani, M. & Devoto, S. (2022) Integrated geomechanical and digital photogrammetric survey in the study of slope instability processes of a flysh sea cliff (Debeli Rtič promontory, Slovenia). *Land*, 11(12), 2255. Available from: https://doi.org/10.3390/land11122255

Furlani, S., Pappalardo, M., Gómez-Pujol, L. & Chelli, A. (2014) Chapter 7 the rock coast of the Mediterranean and black seas. *Geological Society, London, Memoirs*, 40(1), 89–123. Available from: https://doi.org/10.1144/M40.7

Geoportale MASE. (2024) *Geoportale Ministero dell'Ambiente e della Sicurezza Energetica (MASE)*. Piano Straordinario di Telerilevamento Ambientale 2008–2009. Accessed 2024 https://gn.mase.gov.it/portale/home

Geoportale Regione Lazio. (2024) Geoportale Regione Lazio. Carta Geologica 1:25.000. Accessed 2024 https://geoportale.regione.lazio.it/layers/geosdiownr:geonode:carta_geologica_wgs84

Goda, Y., Kudaka, M. & Kawai, H. (2010) Incorporation of Weibull distribution in L-moments method for regional frequency analysis of peaks-over-threshold wave heights. In: *Proceedings of the 32nd International Conference on Coastal Engineering, ASCE, Shanghai, China*.

Himmelstoss, E.A., Henderson, R.E., Farris, A.S., Kratzmann, M.G., Bartlett, M.K., Ergul, A., et al. 2024. Digital shoreline analysis system version 6.0: U.S. geological survey software release. DOI: 10.5066/P13WIZ8M

Hungr, O., Leroueil, S. & Picarelli, L. (2014) The Varnes classification of landslide types, an update. *Landslides*, 11(2), 167–194. Available from: https://doi.org/10.1007/s10346-013-0436-y

Hurst, M.D., Rood, D.H., Ellis, M.A., Anderson, R.S. & Dornbusch, U. (2016) Recent acceleration in coastal cliff retreat rates on the south coast of Great Britain. *Proceedings of the National Academy of Sciences*, 113(47), 13336–13341. Available from: https://doi.org/10.1073/pnas.1613044113

INGV. (2024) Istituto nazionale geofisica e vulcanologia (INGV). Accessed July, 31 2024 https://terremoti.ingv.it/

IPCC. (2021) Climate change 2021: The physical science basis. In: Masson-Delmotte, V., Zhai, P., Pirani, A., Connors, S.L., Péan, C., Berger, S., *et al.* (Eds.) *Contribution of working group I to the sixth assessment report of the intergovernmental panel on climate change*, 1st edition. Cambridge University Press. Accessed October, 25 2023 https://www.cambridge.org/core/product/identifier/9781009157896/type/book

ISPRA. (2024) Istituto Superiore per la Protezione e la Ricerca Ambientale (ISPRA), Rete Mareografica Nazionale (RMN) and Rete Ondametrica Nazionale (RON). Accessed July, 31 2024 https://www.mareografico.it

James, L.A., Hodgson, M.E., Ghoshal, S. & Latiolais, M.M. (2012) Geomorphic change detection using historic maps and DEM differencing: the temporal dimension of geospatial analysis. *Geomorphology*, 137(1), 181–198. Available from: https://doi.org/10.1016/j.geomorph.2010.10.039

Kennedy, D.M., Paulik, R. & Dickson, M.E. (2011) Subaerial weathering versus wave processes in shore platform development: reappraising the old Hat Island evidence. *Earth Surface Processes and Landforms*, 36(5), 686–694. Available from: https://doi.org/10.1002/esp.2092

Leisner, M.M., de Paula, D.P., Alves, D.C.L., da Guia Albuquerque, M., de Holanda Bastos, F. & Vasconcelos, Y.G. (2023) Long-term and short-term analysis of shoreline change and cliff retreat on Brazilian equatorial coast. *Earth Surface Processes and Landforms*, 48(14), 2987–3002. Available from: https://doi.org/10.1002/esp.5668

Lim, M., Strzelecki, M.C., Kasprzak, M., Swirad, Z.M., Webster, C., Woodward, J., et al. (2020) Arctic rock coast responses under a changing climate. *Remote Sensing of Environment*, 236, 111500. Available from: https://doi.org/10.1016/j.rse.2019.111500

Limber, P.W., Barnard, P.L., Vitousek, S. & Erikson, L.H. (2018) A model Ensemble for Projecting Multidecadal Coastal Cliff Retreat during the 21st century. *Journal of Geophysical Research: Earth Surface*, 123(7), 1566–1589. Available from: https://doi.org/10.1029/2017JF004401

Littmann, T. (2000) An empirical classification of weather types in the Mediterranean Basin and their interrelation with rainfall. *Theoretical and Applied Climatology*, 66(3-4), 161–171. Available from: https://doi.org/10.1007/s007040070022

Mancinella, D., Mantero, D. & Testardi, M. (2020) Emissioni gassose sottomarine nel tratto costiero prospiciente Tor Caldara (Lazio meridionale, Italia). *Memorie Descrittive Della Carta Geologica D'italia*, 105, 29–33.

Mancini, M., Bellucci, L. & Petronio, C. (2008) Il Pleistocene Inferiore e Medio di Nettuno (Lazio): stratigrafia e mammalofauna. *Geologica Romana*, 41, 71–85.

Mantero, D. & Giacopini, L. (2020) L'attività estrattiva delle miniere solfifere di Tor Caldara (Anzio, Roma) tra il XVI e il XIX secolo. *Memorie Descrittive Della Carta Geologica D'italia*, 106, 205–2012.

Marmoni, G.M., Martino, S., Censi, M., Menichetti, M., Piacentini, D., Scarascia Mugnozza, G., et al. (2023) Transition from rock mass creep to progressive failure for rockslide initiation at Mt. Conero (Italy). *Geomorphology*, 437, 108750. Available from: https://doi.org/10.1016/j.geomorph.2023.108750

Marra, F., Gaeta, M., Jicha, B.R., Nicosia, C., Tolomei, C., Ceruleo, P., et al. (2019) MIS 9 to MIS 5 terraces along the Tyrrhenian Sea coast of Latium (Central Italy): assessing interplay between sea-level oscillations and tectonic activity. *Geomorphology*, 346, 106843. Available from: https://doi.org/10.1016/j.geomorph.2019.106843

Marra, F., Sevink, J., Tolomei, C., Vannoli, P., Florindo, F., Jicha, B.R., et al. (2023) New age constraints on the MIS 9 – MIS 5.3 marine terraces of the Pontine Plain (central Italy) and implications for global sea levels. *Quaternary Science Reviews*, 300, 107866. Available from: https://doi.org/10.1016/j.quascirev.2022.107866

Martínez, M.L., Intralawan, A., Vázquez, G., Pérez-Maqueo, O., Sutton, P. & Landgrave, R. (2007) The coasts of our world: ecological, economic and social importance. *Ecological Economics*, 63(2-3), 254–272. Available from: https://doi.org/10.1016/j.ecolecon.2006.10.022

Mastronuzzi, G., Aringoli, D., Aucelli, P.P., Baldassarre, M.A., Bellotti, P., Bini, M., et al. (2017) Geomorphological map of the Italian coast: from a descriptive to a morphodynamic approach. *Geografia Fisica e Dinamica Quaternaria*, 40, 161–195. Available from: https://doi.org/10.4461/GFDQ.2017.40.11

Méndez, F.J., Menéndez, M., Luceño, A. & Losada, I.J. (2006) Estimation of the long-term variability of extreme significant wave height using a time-dependent peak Over threshold (POT) model. *Journal of Geophysical Research: Oceans*, 111(C7), 2005JC003344. Available from: https://doi.org/10.1029/2005JC003344

Milli, S., Mancini, M., Moscatelli, M., Stigliano, F., Marini, M. & Cavinato, G.P. (2016) From river to shelf, anatomy of a high-frequency depositional sequence: the late Pleistocene to Holocene Tiber depositional sequence Mohrig D (ed). *Sedimentology*, 63(7), 1886–1928. Available from: https://doi.org/10.1111/sed.12277

Nassar, K., Mahmod, W.E., Fath, H., Masria, A., Nadaoka, K. & Negm, A. (2019) Shoreline change detection using DSAS technique: case of North Sinai coast, Egypt. *Marine Georesources & Geotechnology*, 37(1), 81–95. Available from: https://doi.org/10.1080/1064119X.2018.1448912

Over, J. R., Ritchie, A. C., Kranenburg, C. J., Brown, J.A., Buscombe, D.D., Noble, T. et al. (2021) Processing coastal imagery with Agisoft Metashape Professional Edition, version 1.6— Structure from motion workflow documentation

Pantaloni, M, Crosti, R., Console, F., Nonnis, O., Paganelli, D., Pulcini, M. et al. (2020) Tor Caldara: un itinerario tra geologia, ambiente e storia.

Piacentini, D., Troiani, F., Torre, D. & Menichetti, M. (2021) Land-surface quantitative analysis to investigate the spatial distribution of gravitational landforms along rocky coasts. *Remote Sensing*, 13(24), 5012. Available from: https://doi.org/10.3390/rs13245012

Planet Labs PCB. (2023). Planet imagery product specifications https://earth.esa.int/eogateway/documents/d/earth-online/planet-combined-imagery-product-specs

Poate, T., Masselink, G., Austin, M.J., Dickson, M. & McCall, R. (2018) The role of bed roughness in wave transformation across sloping rock shore platforms. *Journal of Geophysical Research: Earth Surface*, 123(1), 97–123. Available from: https://doi.org/10.1002/2017JF004277

Prémaillon, M., Dewez, T.J.B., Regard, V., Rosser, N.J., Carretier, S. & Guillen, L. (2021) Conceptual model of fracture-limited sea cliff erosion: erosion of the seaward tilted flyschs of Socoa, Basque Country, France. *Earth Surface Processes and Landforms*, 46(13), 2690–2709. Available from: https://doi.org/10.1002/esp.5201

Prémaillon, M., Regard, V., Dewez, T.J.B. & Auda, Y. (2018) GlobR2C2 (global recession rates of coastal cliffs): a global relational database to investigate coastal rocky cliff erosion rate variations. *Earth Surface Dynamics*, 6(3), 651–668. Available from: https://doi.org/10.5194/esurf-6-651-2018

Stark, M., Heckmann, T., Piermattei, L., Dremel, F., Kaiser, A., Machowski, P., et al. (2021) From consumer to enterprise grade: how the choice of four UAS impacts point cloud quality. *Earth Surface Processes and Landforms*, 46(10), 2019–2043. Available from: https://doi.org/10.1002/esp.5142

Štroner, M., Urban, R., Reindl, T., Seidl, J. & Brouček, J. (2020) Evaluation of the Georeferencing accuracy of a photogrammetric model using a Quadrocopter with onboard GNSS RTK. *Sensors*, 20(8), 2318. Available from: https://doi.org/10.3390/s20082318

Strzelecki, M.C., Kasprzak, M., Lim, M., Swirad, Z.M., Jaskólski, M., Pawłowski, Ł., et al. (2017) Cryo-conditioned rocky coast systems: a case study from Wilczekodden, Svalbard. *Science of the Total Environment*, 607–608, 443–453. Available from: https://doi.org/10.1016/j.scitotenv.2017.07.009

Sunamura, T. (1992) *Geomorphology of rocky coasts*. Chichester: J. Wiley.

Sunamura, T. (2015) Rocky coast processes: with special reference to the recession of soft rock cliffs. *Proceedings of the Japan Academy, Series B, Physical and Biological Sciences*, 91(9), 481–500. Available from: https://doi.org/10.2183/pjab.91.481

Torre, D., Galve, J.P., Reyes-Carmona, C., Alfonso-Jorde, D., Ballesteros, D., Menichetti, M., et al. (2024) Geomorphological assessment as basic complement of InSAR analysis for landslide processes understanding. *Landslides*, 21(6), 1273–1292. Available from: https://doi.org/10.1007/s10346-024-02216-w

Trenhaile, A.S. (2011) Cliffs and rock coasts. In: Wolanski, E. & McLusky, D. (Eds.) *Treatise on Estuarine and Coastal Science*, vol. 3. Waltham: Academic Press, pp. 171–191. Available from: https://doi.org/10.1016/B978-0-12-374711-2.00309-0 .

Trigila, A, Iadanza, C., Lastoria, B., Bussettini, M., & Barbano, A. (2021) Dissesto idrogeologico in Italia: pericolosità e indicatori di rischio - Edizione 2021.

Troiani, F., Martino, S., Marmoni, G.M., Menichetti, M., Torre, D., Iacobucci, G., et al. (2020) Integrated field surveying and land surface quantitative analysis to assess landslide proneness in the Conero promontory rocky coast (Italy). *Applied Sciences*, 10(14), 4793. Available from: https://doi.org/10.3390/app10144793

Turner, I.L., Harley, M.D., Almar, R. & Bergsma, E.W. (2021) Satellite optical imagery in coastal engineering. *Coastal Engineering*, 167, 103919. Available from: https://doi.org/10.1016/j.coastaleng.2021.103919

Turner, I.L., Harley, M.D. & Drummond, C.D. (2016) UAVs for coastal surveying. *Coastal Engineering*, 114, 19–24. Available from: https://doi.org/10.1016/j.coastaleng.2016.03.011

Tursi, M.F., Amodio, A.M., Caporizzo, C., Del Pizzo, S., Figliomeni, F.G., Mattei, G., et al. (2023) The response of Sandstone Sea cliffs to Holocene Sea-level rise by means of remote sensing and direct surveys: the case study of Punta Licosa promontory (southern Italy). *Geosciences*, 13(4), 120. Available from: https://doi.org/10.3390/geosciences13040120

Vanneschi, C., Eyre, M., Francioni, M. & Coggan, J. (2017) The use of remote sensing techniques for monitoring and characterization of slope instability. *Procedia Engineering*, 191, 150–157. Available from: https://doi.org/10.1016/j.proeng.2017.05.166

Walkden, M.J.A. & Hall, J.W. (2005) A predictive mesoscale model of the erosion and profile development of soft rock shores. *Coastal Engineering*, 52(6), 535–563. Available from: https://doi.org/10.1016/j.coastaleng.2005.02.005

Young, A.P. & Carilli, J.E. (2019) Global distribution of coastal cliffs. *Earth Surface Processes and Landforms*, 44(6), 1309–1316. Available from: https://doi.org/10.1002/esp.4574

Young, A.P., Guza, R.T., Matsumoto, H., Merrifield, M.A., O'Reilly, W.C. & Swirad, Z.M. (2021) Three years of weekly observations of coastal cliff erosion by waves and rainfall. *Geomorphology*, 375, 107545. Available from: https://doi.org/10.1016/j.geomorph.2020.107545

How to cite this article: Torre, D., Zocchi, M., Iacobucci, G., Menichetti, M., Toselli, R., Troiani, F. et al. (2025) Morphoevolutive drivers on a rapidly-evolving soft rocky cliff and connected shore platform system. *Earth Surface Processes and Landforms*, 50(8), e70117. Available from: https://doi.org/10.1002/esp.70117